generative diseases, these observations suggest that Dorfin may have a significant role in the quality control system in the cell. The present study was designed to obtain further clues for the pathophysiological roles of Dorfin. For this purpose, we screened Dorfin-associated proteins using high performance liquid chromatography coupled to electrospray tandem mass spectrometry (LC-MS/MS). The results showed that Valosin-containing protein (VCP), also called p97 or Cdc48 homologue, obtained from the screening, physically and functionally interacted with Dorfin. Furthermore, both Dorfin and VCP proteins colocalized in aggresomes of the cultured cells and in UBIs in various neurodegenerative diseases.

MATERIALS AND METHODS

Plasmids and Antibodies—pCMV2/FLAG-Dorfin vector (FLAG-Dorfin^{WT}) was prepared by PCR using the appropriate design of PCR primers with restriction sites (ClaI and KpnI). The PCR product was digested and inserted into the ClaI-KpnI site in pCMV2 vector (Sigma). pEGFP-Dorfin (GFP-Dorfin), pCMX-VCP^{Wt} (VCP^{Wt}), and pCMX-VCP^{K524A} (VCP^{K524A}) vectors were described previously (5, 11). pcDNA/HA-VCP^{Wt} (HA-VCP^{Wt}) and pcDNA/HA-VCP^{K524A} (HA-VCP^{K524A}) were subcloned from pCMX-VCP^{Wt} and pCMX-VCP^{K524A}, respectively, into pcDNA3.1 vectors (Invitrogen). The HA tag was introduced at the N terminus of VCP. pcDNA3.1/FLAG-Parkin (FLAG-Parkin) was generated by PCR using the appropriate design of PCR primers with restriction sites (EcoRI and NotI) from pcDNA3.1/Myc-Parkin (12). The FLAG tag was introduced at the N terminus of Parkin. To establish the RING mutant plasmid of Dorfin (FLAG-Dorfin$^{C132S/C135S}$), point mutations for Cys at positions 132 and 135 to Ser were generated by PCR-based site-directed mutagenesis using a QuikChange™ site-directed mutagenesis kit (Stratagene, La Jolla, CA). pcDNA3.1/HA-Ub (HA-Ub), pcDNA3.1/Myc-SOD1^{WT} (SOD1^{WT}-Myc), pcDNA3.1/Myc-SOD1^{G93A} (SOD1^{G93A}-Myc), and pcDNA3.1/Myc-SOD1^{G85R} (SOD1^{G85R}-Myc) were described previously (13, 14). Polyclonal anti-Dorfin (Dorfin-30 and Dorfin-41) and monoclonal anti-VCP antibodies were used as in previous reports (5, 15). The following antibodies were used in this study: monoclonal anti-FLAG antibody (M2; Sigma), monoclonal anti-Myc antibody (9E10; Santa Cruz Biotechnology, Santa Cruz, CA), monoclonal anti-HA antibody (12CA5; Roche Applied Science), polyclonal anti-maltose-binding protein (MBP) antibody (New England BioLabs, Beverly, MA), polyclonal anti-Parkin (Cell Signaling, Beverly, MA), and polyclonal anti-SOD1 (SOD-100; Stressgen, San Diego, CA).

Cell Culture and Transfection—All media and reagents for cell culture were purchased from Invitrogen. HEK293 cells were grown in Dulbecco's modified Eagle's medium containing 10% fetal calf serum, 5 units/ml penicillin, and 50 μg/ml streptomycin. HEK293 cells at subconfluence were transfected with the indicated plasmids using FuGENE6 reagent (Roche Applied Science). To inhibit cellular proteasome activity, cells were treated with 1 μM MG132 (benzyloxycarbonyl-Leu-Leu-Leu-al; Sigma) for 16 h after overnight post-transfection. Cells were analyzed at 24–48 h after transfection.

Protein Identification by LC-MS/MS Analysis—FLAG-Dorfin^{WT} was expressed in HEK293 cells (semiconfluent in a 10-cm dish) and then immunoprecipitated by anti-FLAG antibody. The immunoprecipitates were eluted with a FLAG peptide and then digested with Lys-C endopeptidase (*Achromobacter* protease I). The resulting peptides were analyzed using a nanoscale LC-MS/MS system as described previously (16). The peptide mixture was applied to a Mightysil-PR-18 (1-μm particle, Kanto Chemical Corp., Tokyo) column (45 × 0.150 mm ID) and separated using a 0–40% gradient of acetonitrile containing 0.1% formic acid over 30 min at a flow rate of 50 nl/min. Eluted peptides were sprayed directly into a quadrupole time-of-flight hybrid mass spectrometer (Q-Tof *Ultima*; Micromass, Manchester, UK). MS and MS/MS spectra were obtained in data-dependent mode. Up to four precursor ions above an intensity threshold of 10 cps were selected for MS/MS analysis from each survey scan. All MS/MS spectra were searched against protein sequences of Swiss Prot and RefSeq (NCBI) using batch processes of the Mascot software package (Matrix Science, London, UK). The criteria for match acceptance were the following: 1) when the match score was 10 over each threshold, identification was accepted without further consideration; 2) when the difference of score and threshold was lower than 10 or when proteins were identified based on a single matched MS/MS spectrum, we manually confirmed the raw data prior to acceptance; 3) peptides assigned by less than three y series ions and peptides with +4 charge state were all eliminated regardless of their scores.

Recombinant Proteins and Pull-down Assay—We used pMALp2 (New England BioLabs) and pMALp2T (Factor Xa cleavage site of pMALp2 was replaced with a thrombin recognition site) to express fusion proteins with MBP. To produce the full-length (residues 1–838) Dorfin (MBP-Dorfin^{full}), N-terminal (residues 1–367) Dorfin (MBP-Dorfin^{N}), and C-terminal (residues 368–838) Dorfin (MBP-Dorfin^{C}), the PCR fragments were amplified from pcDNA4/HisMax-Dorfin (4) by using the appropriate PCR primers with restriction sites (FbaI and HindIII) and then ligated into pMAL-p2 vectors. To produce the MBP-Parkin protein, full-length *PARKIN* cDNA was inserted into the EcoRI-NotI sites of pMALp2T. All of the MBP-tagged recombinant proteins were purified from *Escherichia coli* BL21-codon-plus. The detail of the purification method of MBP-tagged proteins was described previously (17). Recombinant GST fusion VCP^{WT} and VCP^{K524A} proteins were also generated from *E. coli* lysate and purified with glutathione-Sepharose. Recombinant His-VCP^{WT} and His-VCP^{K524A} proteins were purified from insect cells using baculovirus. The detail of purification of these recombinant VCP proteins was described previously (15). Binding experiments were performed with proteins carrying different tags. His- or GST-VCP were mixed with MBP fusion proteins: MBP-Dorfin^{full}, -Dorfin^{N}, -Dorfin^{C}, -Parkin, and -mock. His-VCP and GST-VCP proteins were precipitated by Ni^{2+}-nitrilotriacetic acid-agarose (Qiagen, Valencia, CA), and glutathione-Sepharose (Amersham Biosciences), respectively. Binding was performed with 1–3 μg of each protein in 300 μl of binding buffer (50 mM Tris-HCl, pH 7.5, 100 mM NaCl, 5 mM $MgCl_2$, 10% glycerol, 0.5 mg/ml bovine serum albumin, 1 mM dithiothreitol) for 1 h at 4 °C. Then 15 μl of beads were added and incubated for 30 min. The beads were washed by binding buffer three times and eluted with sample buffer and analyzed by SDS-PAGE followed by Western blotting using specific antibodies.

Glycerol Gradient Centrifugation—Cultured cells or mouse tissues were homogenized in 1 ml of PBS with protease inhibitor (Complete Mini; Roche Applied Science). Supernatants (1 mg of protein for cultured cells, 5 mg of protein for mouse tissues, and 0.1 mg of recombinant His-VCP protein) were used as the samples after 10,000 × *g* centrifugation for 20 min. The samples (1.0 ml) were loaded on top of a 34-ml linear gradient of glycerol (10–40%) prepared in 25 mM Tris-HCl buffer, pH 7.5, containing 1 mM dithiothreitol in 40 PA centrifuge tubes (Hitachi, Tokyo), and centrifuged at 4 °C and 80,000 × *g* for 22 h using a Himac CP100α centrifuge system (Hitachi). Thirty fractions were collected from the top of the tubes. Two hundred μl of each fraction was precipitated with acetone, and the remaining pellet was lysed with 50 μl of sample buffer and then used for SDS-PAGE followed by Western blotting.

Immunological Analysis—Cells (4 × 10^5 in a 6-cm dish) were lysed with 500 μl of lysis buffer (50 mM Tris-HCl, 150 mM NaCl, 1% Nonidet P-40, and 1 mM EDTA) with protease inhibitor mixture (Complete Mini) 24–48 h after transfection. The lysate was then centrifuged at 10,000 × *g* for 10 min at 4 °C to remove debris. A 10% volume of the supernatants was used as the "lysate" for SDS-PAGE. When immunoprecipitated, the supernatants were precleared with protein A-Sepharose (Amersham Biosciences), and specific antibodies, anti-FLAG (M2), anti-Myc (9E10), or anti-Dorfin (Dorfin-30) were then added and then incubated at 4 °C with rotation. Immune complexes were then incubated with protein A-Sepharose for 3 h, collected by centrifugation, and washed four times with the lysis buffer. For protein analysis, immune complexes were dissociated by heating in SDS-PAGE sample buffer and loaded onto SDS-PAGE. The samples were separated by SDS-PAGE (12% gel or 4–12% gradient gel) and transferred onto a polyvinylidene difluoride membrane. Finally, Western blotting was performed with specific antibodies.

Immunohistochemistry—HEK293 cells grown on glass coverslips were fixed in 4% paraformaldehyde in PBS for 15 min. Then the cells were blocked for 30 min with 5% (v/v) normal goat serum in PBS, incubated for 1 h at 37 °C with anti-HA antibody (12CA5), washed with PBS, and incubated for 30 min with Alexa 496-nm anti-mouse antibodies (Molecular Probes, Inc., Eugene, OR). The coverslips were washed and mounted on slides. Fluorescence images were obtained using a fluorescence microscope (DMIRE2; Leica, Bannockburn, IL) equipped with a cooled charge-coupled device camera (CTR MIC; Leica). Pictures were taken using Leica Qfluoro software.

Pathological Studies—Pathological studies were carried out on 10% formalin-fixed, paraffin-embedded spinal cords and brain stems filed in the Department of Neurology, Nagoya University Graduate School of Medicine. The specimens were obtained at autopsy from three sporadic cases of ALS and four sporadic PD patients. The spinal cord and brain stem specimens of these ALS and PD cases were immunohistochemically stained with antibodies against Dorfin (Dorfin-41) and VCP. Dou-

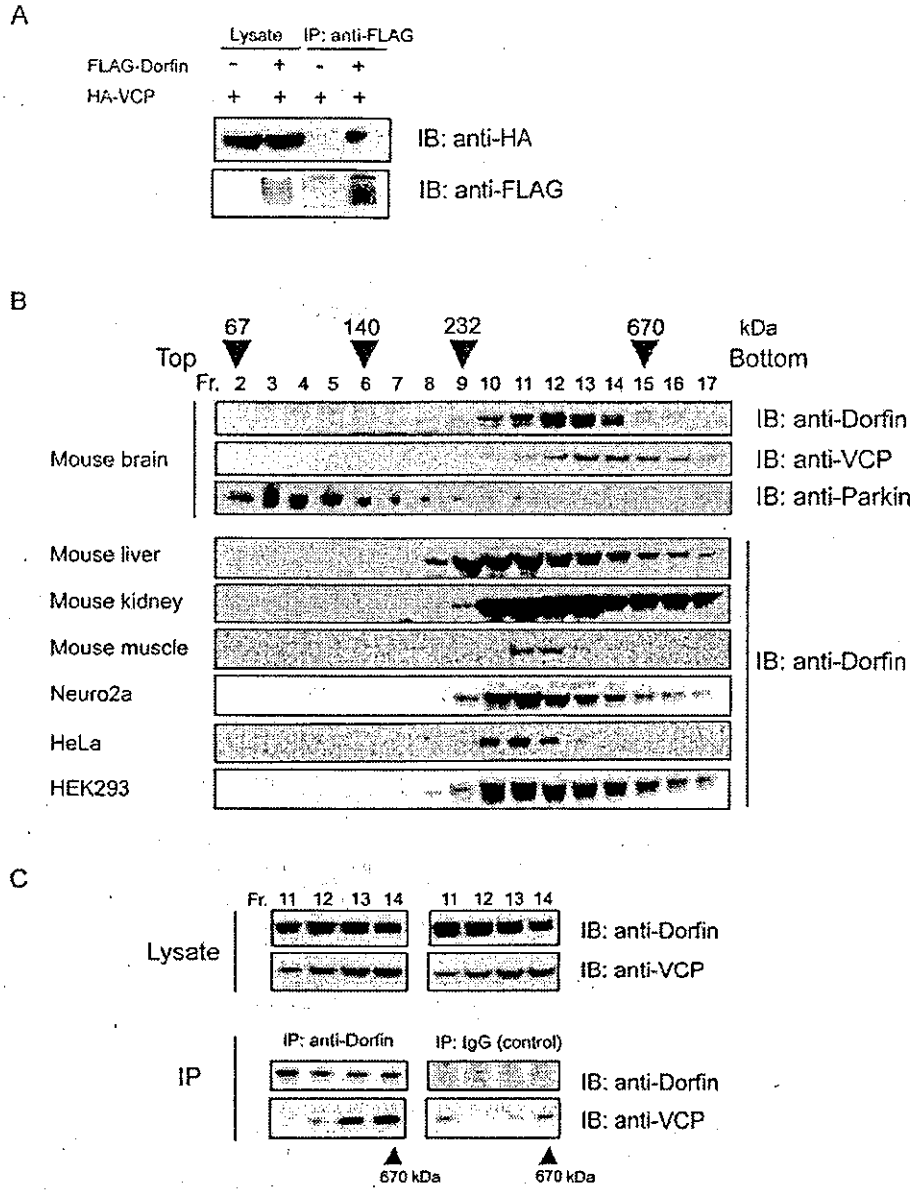

FIG. 1. ***In vivo* interaction between Dorfin and VCP.** *A*, FLAG-Dorfin and HA-VCP are co-expressed in HEK293 cells. FLAG-mock vector was used as a negative control. The amounts of HA-VCP in 10% of the lysate used are shown (*Lysate*); the rest was subjected to immunoprecipitation (*IP*) with anti-FLAG (M2) antibody. Following immunoblotting (*IB*) with anti-HA (12CA5) antibody revealed that HA-VCP was co-immunoprecipitated with FLAG-Dorfin. *B*, 5 mg of protein of various mouse tissues (brain, liver, kidney, and muscle) and 1 mg of protein of cultured cells (HEK293, HeLa, and Neuro2a) were each homogenized in 1 ml of PBS. Supernatants were fractionated by 10–40% glycerol gradient centrifugation followed by separation into 30 fractions using a fraction collector. Immunoblotting using anti-Dorfin, anti-VCP, and anti-Parkin antibodies was performed on the fractions (*Fr.*), including fractions 2–17. Endogenous Dorfin was co-sedimented with VCP in the fractions with a molecular mass of around 400–600 kDa. The positions of co-migrated molecular mass markers are indicated *above* the *panels*. *C*, immunoprecipitation with polyclonal anti-Dorfin antibody (anti-Dorfin-30) was performed on fractions 11–14 collected by glycerol gradient centrifugation analysis, where endogenous Dorfin was seen in *B*. As a negative control, immunoprecipitation with nonimmune rabbit IgG was used on the same fractions.

ble staining of identical sections was performed as described previously (7). In immunofluorescence microscopy, Alexa-488- and Alexa-546-conjugated secondary antibodies (Molecular Probes) were used. All human and animal studies described in this report were approved by the appropriate Ethics Review Committees of the Nagoya University Graduate School of Medicine.

RESULTS

Identification of Dorfin-associated Protein in the Cells—In an effort to identify protein(s) that physically interacts with Dorfin in the cells, FLAG-Dorfin was expressed in HEK293 cells and then immunoprecipitated by anti-FLAG antibody. The immunoprecipitates were eluted with a FLAG peptide and then digested with Lys-C endopeptidase (*Achromobacter* protease I), and the cleaved fragments were directly analyzed using a highly sensitive "direct nanoflow LC-MS/MS" system as described under "Materials and Methods." Following data base search, a total of 13 peptides were assigned to MS/MS spectra obtained from the LC-MS/MS analyses for the FLAG-Dorfin-

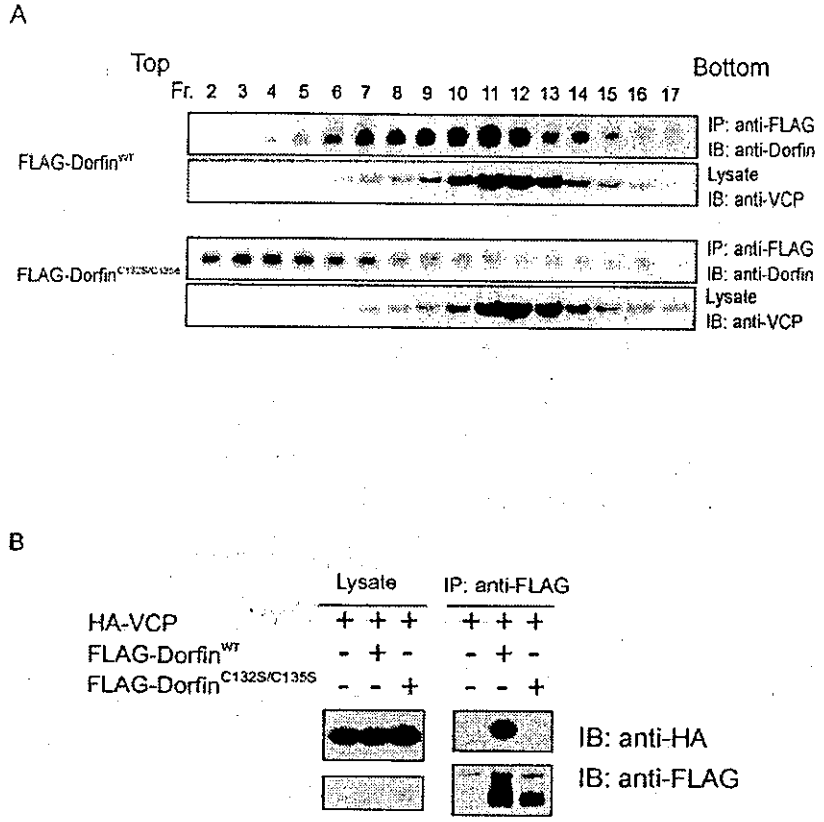

FIG. 2. **Loss of physical interaction between Dorfin$^{C132S/C135S}$ and VCP.** *A*, transfected Dorfin^{WT}, but not Dorfin$^{C132S/C135S}$ (*Dorfin$^{C132S-C135S}$*), forms a high M_r complex. Lysate of HEK293 cells overexpressed with FLAG-Dorfin^{WT} or FLAG-Dorfin$^{C132S/C135S}$ was fractionated by 10–40% glycerol gradient centrifugation. The selected fractions (*Fr.*), fractions 2–17, were subjected to immunoprecipitation (*IP*) using anti-FLAG (M2) antibody. Immunoblotting (*IB*) with anti-Dorfin antibody revealed that exogenous FLAG-Dorfin^{WT} formed a high molecular weight complex, whose peak was at fraction 11, whereas FLAG-Dorfin$^{C132S/C135S}$ migrated in fractions of smaller M_r (around fraction 7). Ten percent of the fractionated samples were shown as "lysate." *B*, Dorfin^{WT} can interact with VCP, but Dorfin$^{C132S/C135S}$ cannot. FLAG-Dorfin^{WT} or FLAG-Dorfin$^{C132S/C135S}$ and HA-VCP were co-expressed in HEK293 cells. FLAG-mock vector was used as a negative control. The amounts of HA-VCP in 10% of the lysate used are shown (*Lysate*); the rest was subjected to immunoprecipitation with anti-FLAG (M2) antibody. Following immunoblotting with anti-HA (12CA5) antibody revealed that HA-VCP was co-immunoprecipitated with FLAG-Dorfin^{WT} but not with FLAG-Dorfin$^{C132S/C135S}$.

associated complexes. These peptide data identified nine proteins as candidates for Dorfin-associated proteins. One of these identified proteins was VCP that has been proposed to have multiple functions, such as membrane fusion or endoplasmic reticulum-associated degradation (ERAD) (18–22). In the next step, we examined the relationship between Dorfin and VCP, because the latter has been reported to be linked to various aspects of neurodegeneration (15).

Dorfin Interacts with VCP in Vivo—To verify the interaction between Dorfin and VCP, FLAG-Dorfin and HA-VCP were transiently overexpressed in HEK 293 cells. Immunological analyses revealed that HA-VCP was co-immunoprecipitated with FLAG-Dorfin but not with FLAG-mock (Fig. 1*A*), confirming their physical interactions in the cells. To determine whether endogenous Dorfin forms a complex, the lysate from mouse brain homogenate was fractioned by glycerol density gradient centrifugation. Each fraction was immunoblotted with anti-Dorfin antibody. The majority of endogenous Dorfin was co-sedimented with VCP around a size of 400–600 kDa, although endogenous Parkin, which is another RING-IBR type E3 ligase (12), existed in the fractions of much lighter molecular weight (M_r) (Fig. 1*B*, *top panels*). Moreover, Dorfin was sedimented in the fractions of 400–600 kDa in other tissues, such as the liver, kidney, and muscle of mouse, and various cultured cells including Neuro2a, HeLa, and HEK293 cells (Fig. 1*B*, *bottom panels*). To determine whether endogenous Dorfin interacts with VCP, immunoprecipitation using polyclonal anti-Dorfin antibody (Dorfin-30) was performed on the fractions shown in Fig. 1*B*, *top panels*. Endogenous VCP was co-immunoprecipitated with endogenous Dorfin in the fractions of high M_r (fractions (*Fr.*) 13 and 14). No apparent band was observed when precipitated with rabbit IgG (Fig. 1*C*).

Mutations of RING Finger Domain of Dorfin Results in Loss of Dorfin-VCP Interactions—Next, we examined whether transfected Dorfin (FLAG-Dorfin^{WT}) and its RING mutant (FLAG-Dorfin$^{C132S/C135S}$), in which the two Cys residues at positions 132 and 135 within the RING finger domain were substituted for Ser residues, form a complex. The results showed overexpression of FLAG-Dorfin^{WT} in high molecular fractions (*Fr.* in Fig. 2), whose peak was between fractions 10 and 12, whereas overexpressed FLAG-Dorfin$^{C132S/C135S}$ did not consist of high molecular weight complex. Overexpression of FLAG-Dorfin^{WT} or FLAG-Dorfin$^{C132S/C135S}$ did not change the sedimentation pattern of VCP (Fig. 2*A*). Furthermore, immunoprecipitation analysis showed that FLAG-Dorfin^{WT}, but not FLAG-Dorfin$^{C132S/C135S}$, could interact with HA-VCP in HEK293 cells (Fig. 2*B*).

Dorfin Interacts with VCP in Vitro—To confirm the direct

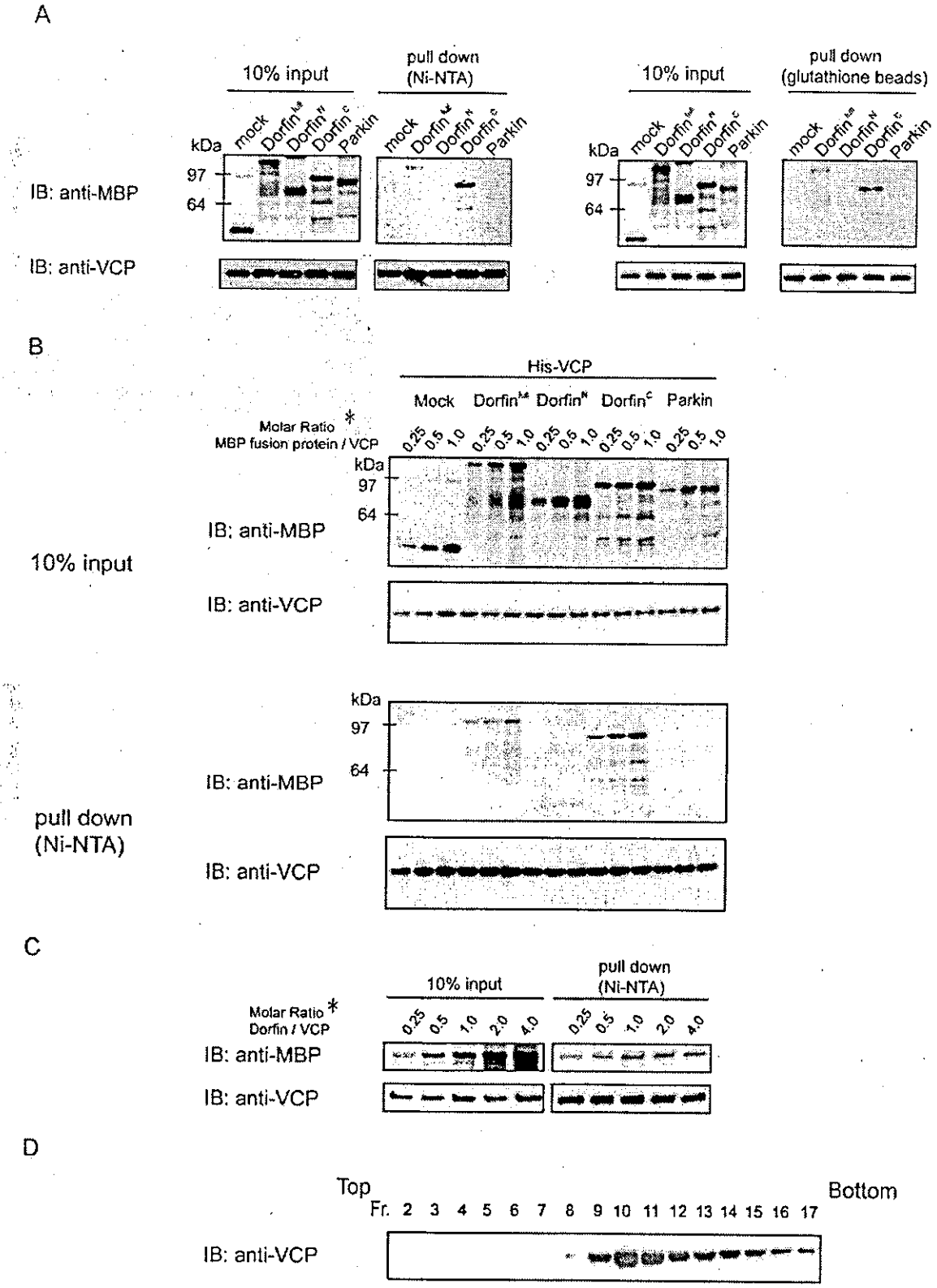

FIG. 3. ***In vitro* interaction between Dorfin and VCP.** *A*, recombinant His- or GST-VCP protein was incubated with MBP-mock, MBP-Dorfin^{full}, MBP-Dorfin^{N}, MBP-Dorfin^{C}, and MBP-Parkin proteins *in vitro*. Two μg of His- or GST-VCP proteins and MBP fusion proteins at similar molar concentrations to VCP proteins were used for the assays. The amounts of MBP fusion and GST fusion Dorfin derivatives and His-VCP in 10% of the samples used are shown (*10% input*). *NTA*, nitrilotriacetic acid. *IB*, immunoblot. *B*, 2 μg of His-VCP was incubated with MBP-mock,

binding between Dorfin and VCP and to determine the exact portion of Dorfin that interacts with VCP *in vitro*, we performed pull-down assays using recombinant proteins. Recombinant MBP-Dorfin or its deletion mutants (*i.e.* MBP-Dorfin^{N} and MBP-Dorfin^{C}) and the same molar of recombinant His-VCP or GST-VCP were mixed and incubated for 1 h at 4 °C. MBP-mock protein was used as a negative control in these experiments. A small portion of MBP-Dorfin^{full} or Dorfin^{C} (C-terminal substrate-recognizing domain) bound to both His-VCP and GST-VCP, whereas MBP-mock, MBP-Dorfin^{N} (N-terminal RING-IBR domain), and MBP-Parkin did not bind to His-VCP or GST-VCP (Fig. 3*A*). We next determined the number of Dorfins that bind one hexamer of VCP. To investigate this issue, we incubated His-VCP with increasing amounts of MBP-Dorfin^{full}, MBP-Dorfin^{N}, MBP-Dorfin^{C}, MBP-mock, or MBP-Parkin. As shown in Fig. 3*B*, the amount of binding portion of MBP-Dorfin^{full} and -Dorfin^{C} pulled down with His-VCP was not saturated below the even molar ratio. The pull-down experiments using excess amounts of MBP-Dorfin^{full} revealed that MBP-Dorfin^{full} was saturated at the even molar ratio (Fig. 3*C*). As reported previously (15), recombinant His-VCP sedimented in high molecular weight fractions, indicating that it formed a hexamer *in vitro* (Fig. 3*D*). These findings indicated that six Dorfin molecules were likely bind to a VCP complex *in vitro*.

Subcellular Localization of Dorfin and VCP in HEK293 Cells—In previous studies, we showed that exogenous and endogenous Dorfin resided perinuclearly and was colocalized with Vimentin in cultured cells treated with a proteasome inhibitor (4). The staining patterns of Dorfin were indistinguishable from those of the aggresome, namely a pericentriolar, membrane-free, cytoplasmic inclusion containing misfolded ubiquitylated proteins packed in a cage of intermediate filaments (4). VCP immunostaining was also observed throughout aggresomes in cultured neuronal cells when induced by treatment with a proteasome inhibitor (15). In order to examine the subcellular localization of Dorfin and VCP, GFP-Dorfin and HA-VCP were co-expressed in HEK293 cells. Without proteasome treatment, GFP-Dorfin-expressing cells showed granular fluorescence in the cytosol, and the HA-VCP-expressing cells showed diffuse and uniform cytoplasmic staining (Fig. 4*A*). Treatment with MG132 (1 μM, 16 h) resulted in accumulation of both GFP-Dorfin and HA-VCP and perinuclear colocalization as a clear large protein aggregate that mimics aggresomes (Fig. 4*B*).

Colocalization of Dorfin and VCP in the Affected Neurons of ALS and PD—In previous studies, immunostaining of Dorfin and VCP was independently noted in LBs of PD, and the peripheral staining pattern of both proteins in LBs was similar (7, 23). To confirm the immunoreactivities of Dorfin and VCP in the affected neurons in ALS and PD, we performed a double-labeling immunofluorescence study using a rabbit polyclonal anti-Dorfin antibody (Dorfin-41) and a mouse monoclonal VCP antibody on the postmortem samples of ALS and PD. In the ALS spinal cords, both proteins were colocalized in the LB-like inclusions (Fig. 5, *A–F*). The margin of LBs in PD was intensely immunostained for Dorfin and VCP, and merged images confirmed their strong colocalization (Fig. 5, *G–L*). Dorfin and VCP were also positive in Lewy neurites in the affected neurons of PD (Fig. 5, *M–O*).

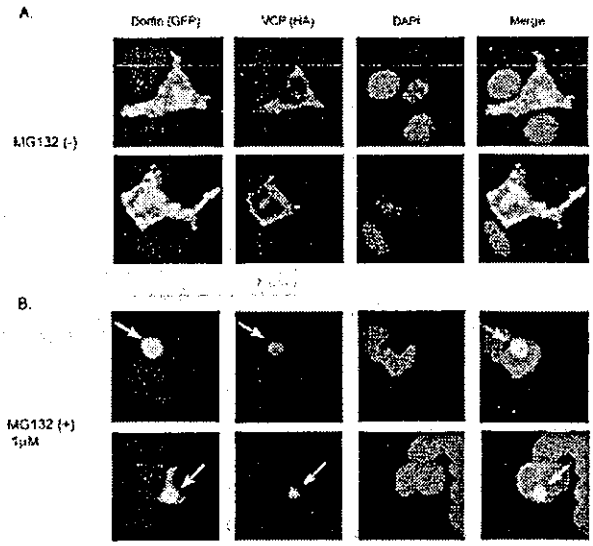

FIG. 4. **Subcellular localization of GFP-Dorfin and HA-VCP in HEK293 cells treated or untreated with a proteasome inhibitor.** GFP-Dorfin and HA-VCP were co-expressed transiently in HEK 293 cells. Cells were treated with (*B*) or without (*A*) 1 μM MG132 for 16 h. HA-VCP was stained with anti-monoclonal HA antibody (12CA5). Nuclei were stained with 4′,6-diamidino-2-phenylindole (*DAPI*). Without the treatment of MG132, GFP-Dorfin was spread through the cytosol, and it appeared like small aggregations. HA-VCP was also seen mainly in the cytosol and partly colocalized with GFP-Dorfin (*A*). After treatment with 1 μM MG132 for 16 h, both GFP-Dorfin and HA-VCP showed perinuclear accumulation and colocalization and appeared as clear large protein aggregates (*B*; *arrows*).

Dorfin Ubiquitylates Mutant SOD1 in Vivo—Unlike the wild-type form, mutant SOD1 proteins are rapidly degraded by the ubiquitin-proteasome system. Consistent with our previous results (5), SOD1^{G93A} and SOD1^{G85R} were polyubiquitylated, and co-expression with FLAG-Dorfin^{WT} enhanced polyubiquitylation of these mutant SOD1s compared with co-expression with FLAG-BAP, a negative control construct (Fig. 6*A*). Boiling with 1% SDS-containing buffer did not change the level of ubiquitylated mutant SOD1, indicating that mutant SOD1 itself was ubiquitylated by Dorfin (Fig. 6*B*). We also performed the same *in vivo* ubiquitylation assay using Neuro2a cells to examine for E3 activity of Dorfin in neuronal cells. The enhanced polyubiquitylation of these mutant SOD1s by Dorfin was observed in Neuro2a cells as well as in HEK293 cells (Fig. 6*C*). FLAG-Dorfin$^{C132S/C135S}$ did not enhance polyubiquitylation of mutant SOD1s, indicating that this RING finger mutant form was functionally inactive (Fig. 6*D*).

VCP^{K524A} Suppresses the E3 Activity of Dorfin—VCP has two ATPase binding domains (D1 and D2). A D2 domain mutant, VCP^{K524A}, induces cytoplasmic vacuoles, which mimics vacuole formation seen in the affected neurons in various neurodegenerative diseases (11, 15). The D2 domain represents the major ATPase activity and is essential for VCP function (11). The ATPase activity of VCP^{K524A} is much lower than that of VCP^{WT}, and VCP^{K524A} caused accumulation of polyubiquitylated proteins in the nuclear and membrane fractions together with elevation of ER stress marker proteins due to ERAD

MBP-Dorfin^{full}, MBP-Dorfin^{N}, MBP-Dorfin^{C}, and MBP-Parkin with increasing amounts (molar ratio to VCP: 0.25, 0.5, and 1.0). The amounts of MBP fusion Dorfin derivatives and His-VCP in 10% of the samples used are shown (10% input). *C*, 2 μg of His-VCP was incubated with MBP-Dorfin^{full} with increasing amounts (molar ratio to VCP: 0.25, 0.5, 1, 2, and 4). The amounts of MBP-Dorfin^{full} and His-VCP in 10% of the samples used are shown (*10% input*). *D*, His-VCP protein (0.5 μg) was fractionated by 10–40% glycerol gradient centrifugation followed by separation into 30 fractions using a fraction collector. Immunoblotting using anti-VCP antibody was performed on the selected fractions (fractions 2–17). *, The molar ratio was calculated by the amount of VCP monomers, not VCP complexes.

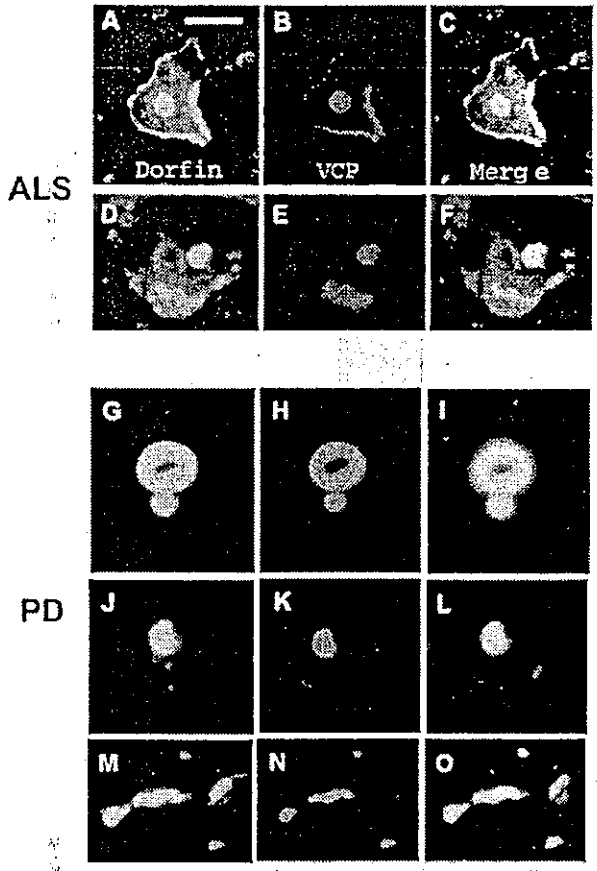

FIG. 5. **Colocalization of Dorfin-41 immunoreactivity with VCP in neuronal inclusions in ALS and PD.** Sections were doubly labeled with anti-Dorfin-41 antiserum and monoclonal VCP antibody and analyzed with a laser-scanning confocal microscope. The *left panels* (*green*) correspond to Dorfin, *middle panels* (*red*) correspond to VCP, and *right panels* correspond to merged images; structures in *yellow* indicate colocalization. Colocalization of Dorfin and VCP is seen in LB-like inclusions in motor neurons of the spinal cord of ALS (*A–F*). Dorfin is also colocalized with VCP in the margin of LBs (*G–I*), premature LBs (*J–L*), and Lewy neurites (*M–O*) in the nigral neurons of PD. *Scale bars*, 20 μm (*A–L*) and 10 μm (*M–O*).

inhibition, whereas its expression level, localization, and complex formation were indistinguishable from those of VCP^{WT} (11). In order to examine the functional effect of VCP on Dorfin, VCP^{WT}, VCP^{K524A}, or LacZ was co-expressed with $SOD1^{G85R}$, FLAG-Dorfin, and HA-Ub in HEK293 cells. Co-expression with VCP^{K524A} showed a marked decline of polyubiquitylation of $SOD1^{G85R}$ compared with co-expression with VCP^{WT} or LacZ (Fig. 7*A*, *top* and *middle*). Since Dorfin physically interacts with mutant SOD1s (5), we next investigated whether this decline of polyubiquitylation of $SOD1^{G85R}$ was mediated by reduced affinity between $SOD1^{G85R}$ and Dorfin. Immunoprecipitation by anti-FLAG antibody showed that VCP^{K524A} did not change affinity between $SOD1^{G85R}$ and Dorfin (Fig. 7*A*, *bottom*). Neither VCP^{WT} nor VCP^{K524A} changed the level of polyubiquitylation protein in the total lysate (Fig. 7*B*). To clarify whether this negative effect of VCP^{K524A} is specific for Dorfin, we assessed the autoubiquitylation of FLAG-Parkin in the presence of VCP^{WT}, VCP^{K524A}, or LacZ. Co-expression of VCP^{K524A} did not decrease autoubiquitylation of FLAG-Parkin compared with co-expression of LacZ or VCP^{WT} (Fig. 7*C*). We performed the same experiments using Neuro2a cells to see whether VCP^{K524A} suppress the E3 activity of Dorfin in neuronal cells. The marked decline of polyubiquitylation of $SOD1^{G85R}$ by VCP^{K524A} expression was also seen in Neuro2a cells (Fig. 7*D*).

DISCUSSION

UBIs in the affected neurons are histopathological hallmarks in various neurodegenerative disorders (8). Dorfin is an E3 ligase, which can ubiquitylate mutant SOD1s and synphilin-1 (5, 24). These substrates and Dorfin were identified in UBIs in various neurodegenerative diseases, such as LB-like inclusions in ALS and LBs in PD and dementia with Lewy bodies (7). This finding suggests that Dorfin may play a crucial role in the process of generating inclusions in the affected neurons. In the present study, we identified VCP as one of the Dorfin-associated proteins using mass spectrometry, and VCP-Dorfin physical interaction was confirmed by an immunoprecipitation experiment using FLAG-Dorfin and HA-VCP overexpressed in HEK293 cells (Fig. 1*A*). VCP is an essential and highly conserved protein of the AAA-ATPase family, which is considered to have diverse cellular functions, such as membrane fusion (25–27), nuclear trafficking (28), cell proliferation (29, 30), and the ERAD pathway (18–22). Many reports have implied that VCP is involved in the pathogenesis of various neuromuscular diseases. VCP has been implicated as a factor that modifies the progress of polyglutamine-induced neuronal cell death (15). In addition, histopathological studies revealed positive staining for VCP in UBIs in PD and ALS with dementia (23). VCP is also associated with MJD protein/atxin-3, in which abnormal expansion of polyglutamine tracts causes Machado-Joseph disease/spinocerebellar ataxia type 3 (31). VCP is also required for the degradation of ataxin-3 in collaboration with E4B/Ufd2a, a ubiquitin chain assembly factor (E4) (32). Recent studies have indicated that missense mutations in the VCP gene cause inclusion body myopathy associated with Paget's disease of bone and frontotemporal dementia, which is characterized by the presence of vacuoles in the cytoplasm in muscle fibers (33).

Our results showed that endogenous Dorfin formed a 400–600-kDa complex in various tissues and various cultured cells (Fig. 1*B*). Dorfin is a ~91-kDa protein; therefore, this high M_r complex should include Dorfin-associated proteins, although the possibility that Dorfin itself oligomerizes in the cell cannot be excluded. Glycerol gradient centrifugation analysis and immunoprecipitation experiments in the present study showed that endogenous Dorfin interacted with endogenous VCP in a complex of approximately 600 kDa, possibly including a Dorfin molecule and a hexametric form of VCP (Fig. 1*C*).

The first RING mutant of Dorfin, in which Cys at positions 132 and 135 changed to Ser, was prepared. This mutant Dorfin, $Dorfin^{C132S/C135S}$, could not ubiquitylate mutant SOD1s (Fig. 6*D*). Glycerol gradient centrifugation analysis revealed that $Dorfin^{C132S/C135S}$ did not form a high M_r complex, whereas exogenous wild type Dorfin ($Dorfin^{WT}$) formed a high M_r complex similar to endogenous Dorfin (Fig. 2*A*). Furthermore, an immunoprecipitation experiment using $Dorfin^{WT}$ and $Dorfin^{C132S/C135S}$ revealed that $Dorfin^{WT}$ could interact with VCP, whereas $Dorfin^{C132S/C135S}$ could not (Fig. 2*B*).

Our *in vitro* study using recombinant proteins showed that full-length ($MBP\text{-}Dorfin^{full}$) and the C terminus of Dorfin ($MBP\text{-}Dorfin^{C}$) directly interacted with VCP, whereas the $MBP\text{-}Dorfin^{N}$ mutant, containing the entire RING finger domain (amino acid residues 1–367), did not bind to VCP (Fig. 3*A*). This finding was unexpected, since *in vivo* binding analysis suggested that Dorfin could interact with VCP at the RING finger domain. It is plausible that certain structural changes in $Dorfin^{C132S/C135S}$ might render the C-terminal VCP-binding portion incapable of accessing VCP molecules. This may explain the result that $Dorfin^{C132S/C135S}$ did not form a high M_r complex.

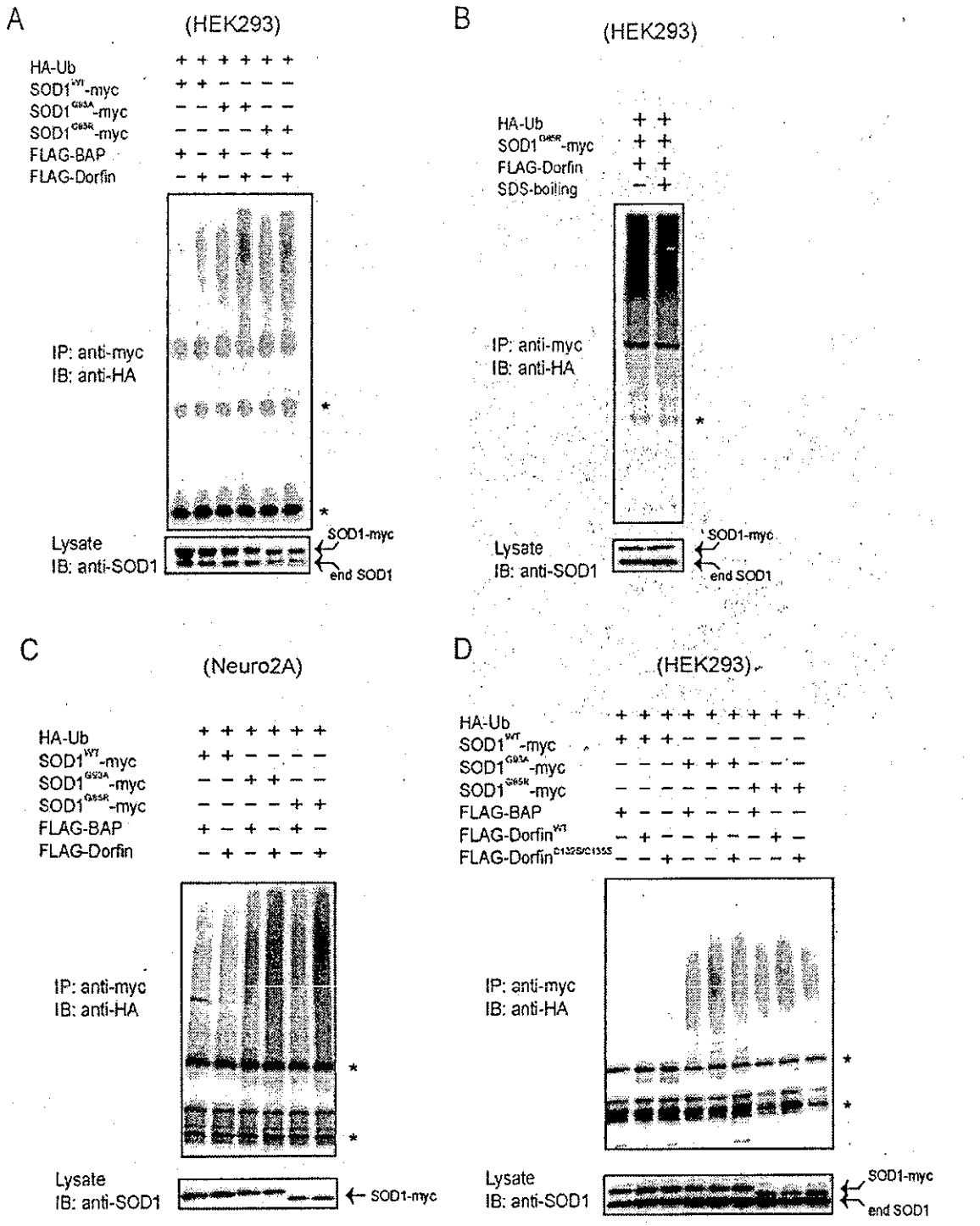

FIG. 6. **Dorfin ubiquitylates mutant SOD1s *in vivo*.** *A*, increased ubiquitylation of mutant SOD1 proteins by overexpression of Dorfin. HEK293 cells were co-transfected with $SOD1^{WT}$-Myc, $SOD1^{G93A}$-Myc, or $SOD1^{G85R}$-Myc and HA-Ub with or without FLAG-Dorfin. FLAG-bovine alkaline phosphatase (*BAP*) was used as a negative control. Immunoprecipitation (*IP*) was performed with Myc antibody (9E10). *IB*, immunoblotting. *B*, SDS boiling was performed prior to immunoprecipitation. To examine covalently ubiquitylated molecules, the cell lysate was boiled with the buffer containing 1% SDS for 5 min. Immunoprecipitation with Myc antibody (9E10) showed that the SDS-boiling procedure did not change polyubiquitylation level of $SOD1^{G85R}$-Myc by Dorfin. *C*, increased ubiquitylation of mutant SOD1 proteins by overexpression of Dorfin in Neuro2a cells. The same *in vivo* ubiquitylation assay as in *A* was performed using Neuro2a cells. *D*, $Dorfin^{C132S/C135S}$ ($Dorfin^{C132S/C135S}$) did not have E3 activity on mutant SOD1. HEK293 cells were co-transfected with $SOD1^{WT}$-Myc, $SOD1^{G93A}$-Myc, or $SOD1^{G85R}$-Myc and HA-Ub with FLAG-$Dorfin^{WT}$ or FLAG-$Dorfin^{C132S/C135S}$. The *asterisks* indicate IgG light and heavy chains.

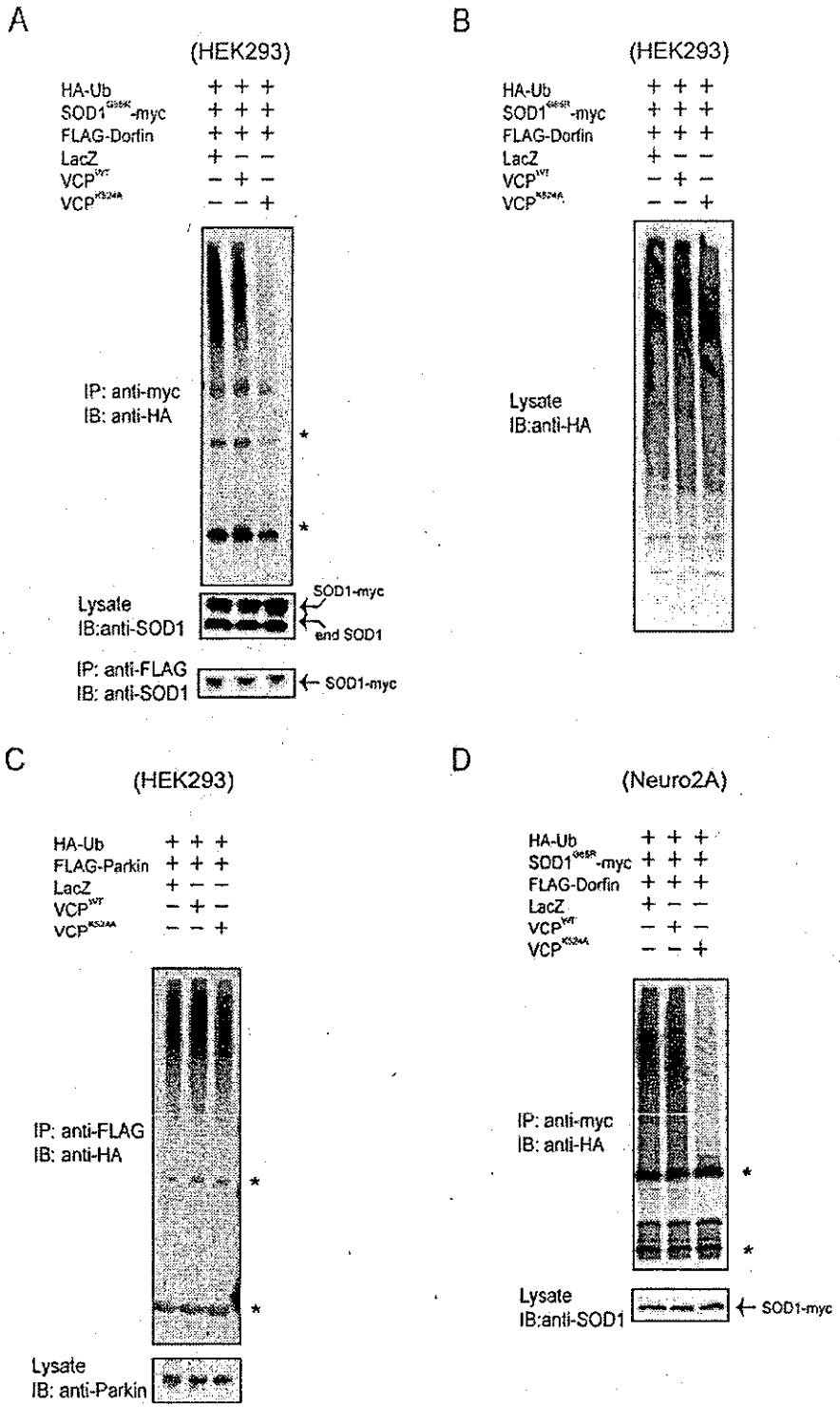

FIG. 7. **A dominant negative mutant of VCP, VCP^{K524A} inhibits the E3 ubiquitin ligase activity of Dorfin.** *A*, inhibition of dominant negative form mutant VCP^{K524A} on the E3 ubiquitin ligase activity of Dorfin. HEK293 cells were co-transfected with SOD1^{G85R}-Myc, HA-Ub, FLAG-Dorfin, and VCP^{WT}, VCP^{K524A}, or LacZ. Immunoprecipitation (*IP*) was performed with Myc antibody (9E10) and FLAG antibody (M2). *IB*, immunoblotting. *B*, neither VCP^{WT} nor VCP^{K524A} changed the level of total polyubiquitylated protein in the cell lysate. Ten percent of the volume of HEK293 cells used in *A* was subjected to immunoblotting using anti-HA (12CA5) antibody. *C*, autoubiquitylation of FLAG-Parkin was not influenced by the dominant negative form VCP^{K524A}. HEK293 cells were co-transfected with FLAG-Parkin, HA-Ub, and VCP^{WT}, VCP^{K524A}, or LacZ. Immunoprecipitation with FLAG antibody (M2) was performed. *D*, inhibition of VCP^{K524A} on E3 ubiquitin ligase activity of Dorfin in Neuro2a cells. Neuro2a cells were co-transfected with SOD1^{G85R}-Myc, HA-Ub, FLAG-Dorfin, and VCP^{WT}, VCP^{K524A}, or LacZ. Immunoprecipitation was performed using Myc antibody (9E10) and FLAG antibody (M2). The *asterisks* indicate IgG light and heavy chains.

The amount of Dorfin bound with VCP was saturated at even molar ratio *in vitro* (Fig. 3, *B* and *C*). Since VCP exists as a homohexamer (Fig. 3*D*), the *in vivo* observed size of ~600 kDa appears to be too small for the Dorfin-VCP complex if one VCP molecule binds to more than one Dorfin as shown in *in vitro* experiments. However, it is noteworthy that the size of molecules estimated by glycerol density gradient centrifugation analysis used in this study is not accurate and sufficient to discuss the molecular interaction of Dorfin and VCP in the cells. To date, various adaptor proteins, with which VCP forms multiprotein complexes, have been identified, such as Npl4, Ufd1 (18, 20), Ufd2 (34), Ufd3 (35), p47 (36), or SVIP (37). Although our *in vitro* study showed direct physical interaction between Dorfin and VCP, the environment with those adaptor proteins might reflect *in vivo* conditions. This also may explain the apparent discrepancy of the Dorfin-VCP binding fashions between *in vivo* and *in vitro* analyses.

Treatment with a proteasomal inhibitor causes the translocation of endogenous VCP and Dorfin to the aggresome in cultured cells (4, 15). Our results showed that these two proteins indeed colocalized perinuclearly in the aggresome following treatment with a proteasomal inhibitor (Fig. 4). Furthermore, we were able to demonstrate both Dorfin and VCP immunoreactivities in LB-like inclusions in ALS and LBs in PD (Fig. 5). In the majority of LBs, indistinguishable peripheral staining patterns were observed with both anti-Dorfin and anti-VCP antibodies. These results confirmed that both Dorfin and VCP are associated with the formation processes of aggresomes and inclusion bodies through physical interaction.

We showed here that co-expression of VCP^{K524A} resulted in a marked decrease of ubiquitylation activity of Dorfin compared with co-expression of VCP^{WT} or control. On the other hand, VCP^{K524A} failed to decrease autoubiquitylation activity of Parkin. VCP^{K524A} did not change the level of polyubiquitylated protein accumulation in the cell lysate in this study (Fig. 7). Knockdown experiments using the RNA interference technique showed accumulation of polyubiquitylated proteins (38). Combined with the observation that inhibition of VCP did not decrease the general accumulation of polyubiquitylated proteins, our results indicated that the E3 regulation function of VCP may be specific to certain E3 ubiquitin ligases such as Dorfin. VCP is an abundant protein that accounts for more than 1% of protein in the cell cytosol and is known to have various chaperone-like activities (39); therefore, it may function as a scaffold protein on the E3 activity of Dorfin. The localization of Dorfin and VCP in UBIs in various neurodegenerative disorders indicates the involvement of these proteins in the quality control system for abnormal proteins accumulated in the affected neurons in neurodegenerative disorders.

Since the unfolded protein response and ERAD are dynamic responses required for the coordinated disposal of misfolded proteins (40), the ERAD pathway can be critical for the etiology of neuronal cell death caused by various unfolded proteins. VCP is required for multiple aspects of the ERAD system by recognition of polyubiquitylated proteins and translocations to the 26 S proteasome for processive degradation through the VCP-Npl4-Ufd1 complex (18, 41). Our results suggest the involvement of Dorfin in the ERAD system, which is related to the pathogenesis of neurodegenerative disorders, such as PD or Alzheimer's disease. Further study including Dorfin knockout and/or knockdown models should examine the pathophysiology of Dorfin in association with the ERAD pathway or other cellular functions. Such studies should enhance our understanding of the pathogenetic role of Dorfin in neurodegenerative disorders.

REFERENCES

1. Julien, J. P. (2001) *Cell* **104**, 581–591
2. Rowland, L. P., and Shneider, N. A. (2001) *N. Engl. J. Med.* **344**, 1688–1700
3. Ishigaki, S., Niwa, J., Ando, Y., Yoshihara, T., Sawada, K., Doyu, M., Yamamoto, M., Kato, K., Yotsumoto, Y., and Sobue, G. (2002) *FEBS Lett.* **531**, 354–358
4. Niwa, J., Ishigaki, S., Doyu, M., Suzuki, T., Tanaka, K., and Sobue, G. (2001) *Biochem. Biophys. Res. Commun.* **281**, 706–713
5. Niwa, J., Ishigaki, S., Hishikawa, N., Yamamoto, M., Doyu, M., Murata, S., Tanaka, K., Taniguchi, N., and Sobue, G. (2002) *J. Biol. Chem.* **277**, 36793–36798
6. Ciechanover, A., and Brundin, P. (2003) *Neuron* **40**, 427–446
7. Hishikawa, N., Niwa, J., Doyu, M., Ito, T., Ishigaki, S., Hashizume, Y., and Sobue, G. (2003) *Am. J. Pathol.* **163**, 609–619
8. Mayer, R. J., Lowe, J., Lennox, G., Doherty, F., and Landon, M. (1989) *Prog. Clin. Biol. Res.* **317**, 809–818
9. Johnston, J. A., Ward, C. L., and Kopito, R. R. (1998) *J. Cell Biol.* **143**, 1883–1898
10. Kopito, R. R. (2000) *Trends Cell Biol.* **10**, 524–530
11. Kobayashi, T., Tanaka, K., Inoue, K., and Kakizuka, A. (2002) *J. Biol. Chem.* **277**, 47358–47365
12. Shimura, H., Hattori, N., Kubo, S., Mizuno, Y., Asakawa, S., Minoshima, S., Shimizu, N., Iwai, K., Chiba, T., Tanaka, K., and Suzuki, T. (2000) *Nat. Genet.* **25**, 302–305
13. Fukuchi, M., Imamura, T., Chiba, T., Ebisawa, T., Kawabata, M., Tanaka, K., and Miyazono, K. (2001) *Mol. Biol. Cell* **12**, 1431–1443
14. Ishigaki, S., Liang, Y., Yamamoto, M., Niwa, J., Ando, Y., Yoshihara, T., Takeuchi, H., Doyu, M., and Sobue, G. (2002) *J. Neurochem.* **82**, 576–584
15. Hirabayashi, M., Inoue, K., Tanaka, K., Nakadate, K., Ohsawa, Y., Kamei, Y., Popiel, A. H., Sinohara, A., Iwamatsu, A., Kimura, Y., Uchiyama, Y., Hori, S., and Kakizuka, A. (2001) *Cell Death Differ.* **8**, 977–984
16. Natsume, T., Yamauchi, Y., Nakayama, H., Shinkawa, T., Yanagida, M., Takahashi, N., and Isobe, T. (2002) *Anal. Chem.* **74**, 4725–4733
17. Matsuda, N., Suzuki, T., Tanaka, K., and Nakano, A. (2001) *J. Cell Sci.* **114**, 1949–1957
18. Bays, N. W., and Hampton, R. Y. (2002) *Curr. Biol.* **12**, R366–R371
19. Ye, Y., Meyer, H. H., and Rapoport, T. A. (2001) *Nature* **414**, 652–656
20. Braun, S., Matuschewski, K., Rape, M., Thoms, S., and Jentsch, S. (2002) *EMBO J.* **21**, 615–621
21. Jarosch, E., Taxis, C., Volkwein, C., Bordallo, J., Finley, D., Wolf, D. H., and Sommer, T. (2002) *Nat. Cell Biol.* **4**, 134–139
22. Rabinovich, E., Kerem, A., Frohlich, K. U., Diamant, N., and Bar-Nun, S. (2002) *Mol. Cell. Biol.* **22**, 626–634
23. Mizuno, Y., Hori, S., Kakizuka, A., and Okamoto, K. (2003) *Neurosci. Lett.* **343**, 77–80
24. Ito, T., Niwa, J., Hishikawa, N., Ishigaki, S., Doyu, M., and Sobue, G. (2003) *J. Biol. Chem.* **278**, 29106–29114
25. Meyer, H. H., Kondo, H., and Warren, G. (1998) *FEBS Lett.* **437**, 255–257
26. Kondo, H., Rabouille, C., Newman, R., Levine, T. P., Pappin, D., Freemont, P., and Warren, G. (1997) *Nature* **388**, 75–78
27. Rabouille, C., Kondo, H., Newman, R., Hui, N., Freemont, P., and Warren, G. (1998) *Cell* **92**, 603–610
28. Hetzer, M., Meyer, H. H., Walther, T. C., Bilbao-Cortes, D., Warren, G., and Mattaj, I. W. (2001) *Nat. Cell Biol.* **3**, 1086–1091
29. Frohlich, K. U., Fries, H. W., Rudiger, M., Erdmann, R., Botstein, D., and Mecke, D. (1991) *J. Cell Biol.* **114**, 443–453
30. Asai, T., Tomita, Y., Nakatsuka, S., Hoshida, Y., Myoui, A., Yoshikawa, H., and Aozasa, K. (2002) *Jpn. J. Cancer Res.* **93**, 296–304
31. Kawaguchi, Y., Okamoto, T., Taniwaki, M., Aizawa, M., Inoue, M., Katayama, S., Kawakami, H., Nakamura, S., Nishimura, M., Akiguchi, I., Kimura, J., Narumiya, S., and Kakizuka, A. (1994) *Nat. Genet.* **8**, 221–228
32. Matsumoto, M., Yada, M., Hatakeyama, S., Ishimoto, H., Tanimura, T., Tsuji, S., Kakizuka, A., Kitagawa, M., and Nakayama, K. I. (2004) *EMBO J.* **23**, 659–669
33. Watts, G. D., Wymer, J., Kovach, M. J., Mehta, S. G., Mumm, S., Darvish, D., Pestronk, A., Whyte, M. P., and Kimonis, V. E. (2004) *Nat. Genet.* **36**, 377–381
34. Koegl, M., Hoppe, T., Schlenker, S., Ulrich, H. D., Mayer, T. U., and Jentsch, S. (1999) *Cell* **96**, 635–644
35. Ghislain, M., Dohmen, R. J., Levy, F., and Varshavsky, A. (1996) *EMBO J.* **15**, 4884–4899
36. Meyer, H. H., Wang, Y., and Warren, G. (2002) *EMBO J.* **21**, 5645–5652
37. Nagahama, M., Suzuki, M., Hamada, Y., Hatsuzawa, K., Tani, K., Yamamoto, A., and Tagaya, M. (2003) *Mol. Biol. Cell* **14**, 262–273
38. Wojcik, C., Yano, M., and DeMartino, G. N. (2004) *J. Cell Sci.* **117**, 281–292
39. Dalal, S., and Hanson, P. I. (2001) *Cell* **104**, 5–8
40. Travers, K. J., Patil, C. K., Wodicka, L., Lockhart, D. J., Weissman, J. S., and Walter, P. (2000) *Cell* **101**, 249–258
41. Dai, R. M., and Li, C. C. (2001) *Nat. Cell Biol.* **3**, 740–744

THE JOURNAL OF BIOLOGICAL CHEMISTRY
© 2004 by The American Society for Biochemistry and Molecular Biology, Inc.

Vol. 279, No. 51, Issue of December 17, pp. 53427–53434, 2004
Printed in U.S.A.

An RNA-interacting Protein, SYNCRIP (Heterogeneous Nuclear Ribonuclear Protein Q1/NSAP1) Is a Component of mRNA Granule Transported with Inositol 1,4,5-Trisphosphate Receptor Type 1 mRNA in Neuronal Dendrites*[S]

Received for publication, August 24, 2004, and in revised form, October 5, 2004
Published, JBC Papers in Press, October 8, 2004, DOI 10.1074/jbc.M409732200

Hiroko Bannai‡§, Kazumi Fukatsu§, Akihiro Mizutani‡¶, Tohru Natsume‖, Shun-ichiro Iemura‖, Tohru Ikegami§, Takafumi Inoue§¶, and Katsuhiko Mikoshiba‡§¶‡‡**

From the ‡Laboratory for Developmental Neurobiology, Brain Science Institute, RIKEN, 2-1 Hirosawa, Wako, Saitama 351-0198, Japan, §Division of Molecular Neurobiology and ‡‡Division of Neural Signal Information NTT-IMSUT, The Institute of Medical Science, The University of Tokyo, 4-6-1 Shirokanedai, Minato-ku, Tokyo 108-8639 Japan, ¶Calcium Oscillation Project, ICORP, Japan Science and Technology Corp., 3-4-4 Shirokanedai, Minato-ku, Tokyo 108-0071, Japan, and ‖National Institute of Advanced Industrial Science and Technology, Biological Information Research Center, 2-41-6 Ohmi, Kohtoh-ku, Tokyo 135-0064, Japan

mRNA transport and local translation in the neuronal dendrite is implicated in the induction of synaptic plasticity. Recently, we cloned an RNA-interacting protein, SYNCRIP (heterogeneous nuclear ribonuclear protein Q1/NSAP1), that is suggested to be important for the stabilization of mRNA. We report here that SYNCRIP is a component of mRNA granules in rat hippocampal neurons. SYNCRIP was mainly found at cell bodies, but punctate expression patterns in the proximal dendrite were also seen. Time-lapse analysis in living neurons revealed that the granules labeled with fluorescent protein-tagged SYNCRIP were transported bi-directionally within the dendrite at ~0.05 μm/s. Treatment of neurons with nocodazole significantly inhibited the movement of green fluorescent protein-SYNCRIP-positive granules, indicating that the transport of SYNCRIP-containing granules is dependent on microtubules. The distribution of SYNCRIP-containing granules overlapped with that of dendritic RNAs and elongation factor 1α. SYNCRIP was also found to be co-transported with green fluorescent protein-tagged human staufen1 and the 3′-untranslated region of inositol 1,4,5-trisphosphate receptor type 1 mRNA. These results suggest that SYNCRIP is transported within the dendrite as a component of mRNA granules and raise the possibility that mRNA turnover in mRNA granules and the regulation of local protein synthesis in neuronal dendrites may involve SYNCRIP.

Protein synthesis in neurons was long believed to occur only in the cell body, but recent evidence showing the presence of mRNA (for review, see Refs. 1–4) and the capacity for local translation of specific mRNAs in neuronal dendrites (Refs. 5 and 6; for review, see Refs. 7 and 8) has changed this belief. Selective transport and localization of certain types of mRNA and subsequent local protein synthesis in neuronal dendrites are now considered as part of the fundamental mechanisms involved in synaptic plasticity.

Various kinds of mRNA, such as mRNA-coding cytoskeletal proteins (MAP2, β-actin, Arc (activity-regulated cytoskeleton-associated protein), and neurofilament proteins), kinases (*e.g.* the α subunit of Ca^{2+}/CaM[1] kinase II (CaMKIIα)), receptors and channels (glycine receptors, glutamate receptors, and inositol 1,4,5-trisphosphate receptor type 1 (IP_3R1)) have been reported to target dendrites of central nervous system neurons (for review, see Refs.4, 8). Many of the mRNAs listed above are transported to the dendrites as a component of ribonucleoprotein complexes called mRNA granules, which were detected with fluorescent dye SYTO14 (9) and by the *in situ* hybridization technique (10, 11). mRNA granules contain ribosomes and other components of translational machinery (9, 12, 13) as well as various mRNA-binding proteins, including fragile X mental retardation protein (14), staufen (15), testis-brain RNA-binding protein (16), zip code-binding protein 1 (17), and heterogeneous nuclear ribonuclear protein (hnRNP) A2 (18). These mRNA-binding proteins are thought to be responsible for the stability and the translational regulation of mRNAs; however, their actual function in dendrites is poorly understood.

We recently discovered a novel RNA-interacting protein, SYNCRIP (synaptotagmin binding, cytoplasmic RNA-interacting protein (19)) in mouse. A human homolog of SYNCRIP was termed as NSAP1 (20) or hnRNP Q1 (21). SYNCRIP is one of three alternative splicing variants (21) and has high homology to hnRNP R. Interestingly, in contrast to hnRNP R and other splicing variants of SYNCRIP (hnRNP Q2 and Q3), SYNCRIP is distributed throughout the cytosol instead of being localized in the nucleus (19). SYNCRIP binds to RNA *in vitro*, preferen-

* This study was supported by grants from the Ministry of Education, Culture, Sports, Science, and Technology (MEXT) of Japan (to T. Inoue and K. M.), the Ministry of Health, Labor, and Welfare of Japan (to T. Inoue), and the 21st Century Center of Excellence Program, Center for Integrated Brain Medical Science from MEXT of Japan (to K. F.). The costs of publication of this article were defrayed in part by the payment of page charges. This article must therefore be hereby marked "*advertisement*" in accordance with 18 U.S.C. Section 1734 solely to indicate this fact.

[S] The on-line version of this article (available at http://www.jbc.org) contains supplemental Table SI, supplemental Data S1, and the legends for supplemental Movies 1–3.

** To whom correspondence should be addressed: Division of Molecular Neurobiology, The Institute of Medical Science, The University of Tokyo, 4-6-1 Shirokanedai, Minato-Ku, Tokyo, 108-8639, Japan. Tel.: 81-3-5449-5320; Fax: 81-3-5449-5420; E-mail: tinoue@ims.u-tokyo.ac.jp.

[1] The abbreviations used are: CaM, calmodulin; CaMKIIα, α subunit of Ca^{2+}/CaM kinase II; IP_3R1, inositol 1,4,5-trisphosphate receptor type 1; hnRNP, heterogeneous nuclear ribonuclear protein; SYNCRIP, synaptotagmin binding cytoplasmic RNA-interacting protein; PBS, phosphate-buffered saline; GFP, green fluorescent protein; mRFP, monomeric red fluorescent protein; NLS, nuclear localization signal; 3′-UTR, 3′-untranslated region; MS2bs, MS2 phage coat protein binding sequences; EF1α, elongation factor1α; EtBr, ethidium bromide; CCD, charge-coupled device; A2RE, hnRNP A2 response element.

tially to poly (A) or poly (U), in a phosphorylation-dependent manner (19, 22, 23). Although SYNCRIP is reported to be a component of protein complexes that stabilize c-*fos* proto-oncogene mRNA in mammalian culture cells (24), the physiological role of SYNCRIP in the cytoplasm is not yet understood. In this study we performed a proteomic analysis of the protein complexes that associate with SYNCRIP in human kidney cell line 293EBNA and found that SYNCRIP preferentially associated with ribosomal proteins and RNA-binding proteins. We also found that SYNCRIP is a component of mRNA granules containing IP_3R1 mRNA transported within the dendrites in a microtubule-dependent manner.

EXPERIMENTAL PROCEDURES

Proteomic Analysis—Proteomics analysis of the proteins that associate with SYNCRIP was performed as previously described (25–27). In brief, human 293EBNA cells were harvested, washed with phosphate-buffered saline (PBS), and lysed at 24 h after the transfection of cDNA coding FLAG-tagged SYNCRIP. Then the resulting cell lysate was incubated with M2-agarose overnight at 4 °C for immunoprecipitation. The protein-bound agarose beads were washed extensively, and the proteins were eluted with FLAG peptide. The isolated complex was precipitated using mixed methanol and chloroform. After vacuum-drying, the precipitate was digested with *Achromobacter* protease I. The digested peptide mixture were analyzed using a Direct nano flow LC-MSM system as described (26), and protein identification was performed according to the criteria described previously (26).

Construction of Fusion Proteins—FLAG-tagged SYNCRIP was generated by subcloning PCR-amplified DNA fragment coding mouse SYNCRIP (19) fused with FLAG tag to its N terminus into pcDNA3 (Invitrogen). To construct a green fluorescent protein (GFP)-tagged SYNCRIP, the coding sequence of mouse SYNCRIP was subcloned into the PstI/KpnI site of pEGFP-C3 (Clontech, Palo Alto, CA). Monomeric red fluorescent protein (mRFP)-tagged SYNCRIP (mRFP-SYNCRIP) was generated by fusing a mRFP, a gift from Dr. R. Tsien (28), to the N terminus of SYNCRIP with the amino acids Glu-Phe as a linker, which was then subcloned into pcDNA3.1/Zeo+ (Invitrogen). To construct GFP-fused human staufen1 (GFP-hStau1), the coding region of hStau1 was amplified from HEP22160 (a gift from Dr. S. Sugano) and subcloned into the XhoI/HindIII site of pEGFP-C1 (Clontech).

NLS-MS2-Venus was generated from pGA14-MS2-GFP (a gift from Dr. R. Singer (29)) and pCS2-Venus (a gift from Dr. A. Miyawaki). A coding sequence of "Venus" (a variant of yellow fluorescent protein (30)) was PCR-amplified with 5′-GTGCGGCCGCTGGTATGAGCAAGGGCGAGG-3′and 5′-CTTGAATTCTTACTTGTACAG-3′ using pCS2-Venus as a template. The NotI-EcoRI digest of the resultant cDNA fragment and the BamHI-NotI digest of pG14-MS2-GFP that corresponded to the coding sequence of MS2 coat protein and nuclear localization signal (NLS) were then introduced into the BamHI/EcoRI site of a mammalian expression vector pCS2+.

To construct the RNA expression vector of the 3′-untranslated regions (3′-UTR) of IP_3R1 (IP_3R1 3′-UTR-MS2bs), we amplified a cDNA fragment of 3′-UTR of mouse IP_3R1 (bases 8579–9041) by PCR using primers 5′-GGCTCGAGGCAAATGAGGCAGAGGGAC-3′, and 5′-GCGGGCCCAACCATTTATTACACGAGTATCAAC-3′. The resulting PCR fragment was subcloned into the XhoI/ApaI site of pcDNA3.1/Zeo+, upstream of which 12 copies of MS2 phage coat protein binding sequences (MS2bs) and the coding sequence of alkaline phosphatase were inserted, and the bovine growth hormone polyadenylation signal downstream to the multicloning site was removed.

Cell Culture and Transfection—Primary cultures of neurons were prepared from hippocampi of 1-day-old Wistar rats by a standard method as described previously (31, 32) and plated on poly-L-lysine (Nacalai Tesque, Kyoto, Japan)-coated coverslips at a density of 4.6×10^4-1.3×10^5 cells/cm^2. Cells were cultured in Neurobasal medium (Invitrogen) supplemented with 2.5 mM L-glutamine (Nacalai Tesque), 2.5% (v/v) B-27 (Invitrogen), and antibiotics (250 units/ml penicillin and 250 μg/ml streptomycin). The cultures were transfected with 10 μg of DNAs by a standard calcium phosphate method (33) or 2.5 μg of DNAs by lipofection using Lipofectamine 2000 (Invitrogen) (34) on days 5–6 *in vitro*. For the labeling of 3′-UTR of IP_3R1 mRNA, 0.6 μg of NLS-MS2-Venus and 1.8 μg of IP_3R1 3′-UTR-MS2bs were co-transfected by lipofection. The transfected cells were used for immunohistochemistry or imaging experiments 2–3 days after the transfection, which corresponded to days 7–9 *in vitro*.

Antibodies—The rabbit antibody recognizing the N-terminal region of SYNCRIP, anti-SYNCRIP-N antibody, was obtained as described previously (19). Anti-SYNCRIP-N was used after affinity purification, and the specificity of this antibody has been confirmed by parallel experiments using preimmune serum or anti-SYNCRIP-N antibody preincubated with an excess amount of antigenic polypeptide (19). Anti-elongation factor1α (EF1α) antibody was from Upstate Biotechnology (Charlottesville, VA, clone CBP-KK1). Alexa 488- or Alexa 594-conjugated secondary antibody was from Molecular Probes (Eugene, OR).

Immunohistochemistry, Cell Labeling Experiments, and Confocal Imaging—For immunohistochemistry of native hippocampus, Wistar rats were deeply anesthetized on postnatal day 7 and perfused with 4% paraformaldehyde in PBS. Whole brains were removed and post-fixed in the same fixative overnight at 4 °C. Sagittal sections (thickness, 100 μm) were cut with a Vibratome-type micro slicer (DTK-1500; Dosaka EM, Kyoto, Japan), collected in PBS, and permeabilized with 0.3% Triton X-100. After incubating with blocking solution (1% bovine serum albumin and 0.3% Triton X-100 in PBS) sections were incubated with anti-SYNCRIP-N antibody (1:1000 dilution) in blocking solution overnight at 4 °C and subsequently with Alexa 488-conjugated anti rabbit IgG (Molecular Probes) for 3 h at room temperature. Finally, sections were mounted on slides with Vectashield (Vector Laboratories, Burlingame, CA) and observed under a confocal-scanning microscope (FV-300; Olympus, Tokyo, Japan) attached to an inverted microscope (IX70; Olympus) with a ×10 objective (NA 0.30; Olympus) and a ×40 objective (NA 0.85; Olympus).

For immunostaining of cultured neurons, cells were fixed with 4% formaldehyde in PBS for 10 min. After permeabilization with 0.1% Triton X-100 in PBS for 10 min and blocking with 5% skim milk in PBS, the cells were incubated with the primary antibodies at 1:1000 dilution for anti-SYNCRIP-N antibody and at 1:400 dilution for anti-EF1α antibody. Alexa 488- or Alexa 594-conjugated IgGs (Molecular Probes) were used as secondary antibodies. RNA labeling with ethidium bromide (EtBr) was performed as described previously (35). RNase treatment was conducted by incubating neurons with 20 μg/ml RNase A (Nippongene, Tokyo, Japan) for 15 min after the EtBr staining. For labeling hippocampal neurons with endosomal and lysosomal markers, cells were incubated with 1 mg/ml Texas Red-dextran (M_r 3000; Molecular Probes) overnight. Fluorescence images of cultured neurons were taken under a confocal-scanning microscope (FV-300) using a 60× objective (NA 1.4; Olympus).

All of the images taken by the confocal microscope were digitally smoothed to reduce the noise level. The smoothing filter was implemented using 3 × 3 spatial convolutions, where the value of each pixel in the selection was replaced with the weighted average of its 3 × 3 neighborhood. Center pixels are 4-fold weighted over surrounding pixels.

Time-lapse Imaging and Data Analysis—The culture medium was supplemented with 20 mM HEPES (pH 7.3) for the time-lapse imaging experiments. The temperature was maintained at ~37 °C by a heating chamber that surrounded the microscope stage. For single color time-lapse imaging, the cells were visualized under an inverted microscope (IX70, Olympus) and a 60× objective (NA 1.45, Olympus) using standard filter sets and a mercury lamp. Sequential images were acquired with a cooled charge-coupled device (CCD) camera (ORCA-ER; Hamamatsu Photonics, Hamamatsu, Japan) with a 58- or 117-ms exposure time every 10 s. For multicolor time-lapse imaging, neurons were visualized under an inverted microscope (IX81; Olympus) equipped with a motorized fluorescence mirror unit exchanger, standard filter sets, and a 60× objective (NA 1.4; Olympus). Images were taken with a cooled CCD camera (ORCA-ER) with a 200-ms exposure time every 10 s.

Data were analyzed using TI Workbench, which is a custom-made software written by T. Inoue. Positions of fluorescent vesicles were plotted against time, and velocity of the granular movements was obtained by linear fitting of the slope. Only structures moving in more than three image frames were taken into account. The velocities were calculated for each period of consecutive movement. Images of time-lapse (Figs. 3*A*, 6*B*, and 7*C*) presented in this study were subjected to digital smoothing with the same algorithm as the confocal images (see above) to reduce the noise level.

Drug Preparation and Drug Treatment—Stock solutions of nocodazole (10 mg/ml, Sigma) and latrunculin A (1 mg/ml, Molecular Probes) were prepared in dimethyl sulfoxide (Me_2SO) and stored at −20 °C. Neurons were incubated with nocodazole (30 μg/ml) and latrunculin A (1 μg/ml) for 1 h at 37 °C in 5% CO_2. To confirm that the cytoskeleton was disrupted, fixed cells were stained with anti-tubulin antibody (Lab Vision, CA) or Alexa 594-phalloidin (Molecular Probes). We found no

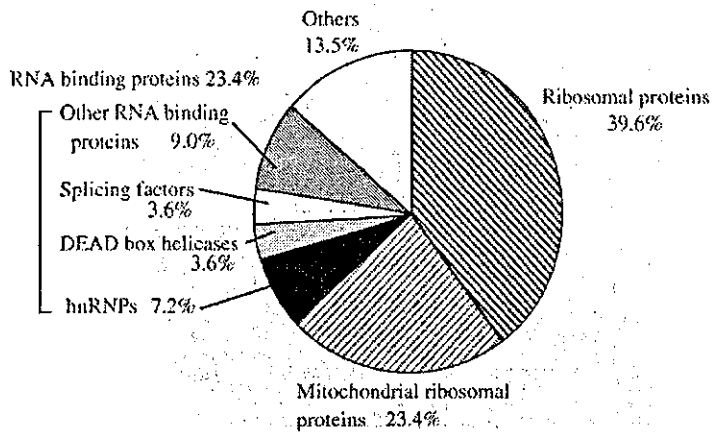

FIG. 1. **Classification of the 111 proteins identified as components of the SYNCRIP-associated protein complexes in 293EBNA cells.** Detailed compositions of each class are shown in supplemental Table SI.

changes in the microtubules or actin structure from control cells exposed to 0.1–0.3% Me_2SO (data not shown).

RESULTS

Proteomic Analysis of SYNCRIP-associated Proteins—Proteins associated with SYNCRIP were isolated by immunoprecipitation from human 293EBNA cells expressing FLAG-tagged SYNCRIP by using anti-FLAG antibody. The 111 proteins listed in supplemental Table SI were identified as components of protein complexes containing FLAG-tagged SYNCRIP. Among these 111 proteins, 44 were identified as ribosomal proteins (39.6%) and 26 were mitochondrial ribosomal proteins (23.4%), which are encoded by nuclear genes and synthesized in the cytosol (36) (Fig. 1 and supplemental Table SI). In addition, 26 RNA-binding proteins (23.4%) including 8 hnRNPs (7.2%), 4 DEAD box helicases (3.6%), and 4 splicing factors (3.6%) were also identified as SYNCRIP-associated proteins. These results suggest that SYNCRIP preferentially associates with protein complexes involved in mRNA processing and translation.

The Distribution and Dynamics of SYNCRIP in Hippocampal Neurons—mRNA granules, the ribonucleoprotein complexes present in neuronal dendrites, have been reported to contain ribosomes and other components of translation machinery (9, 12, 13) as well as a number of RNA-binding proteins (14–18). The above results of proteomic analysis in 293EBNA cells indicate that SYNCRIP preferentially associates with the major component of mRNA granules, that is, ribosomal proteins and RNA-binding proteins (Fig. 1, supplemental Table SI). In addition, SYNCRIP itself has the ability to bind to RNA, preferentially to poly(A) and poly(U) sequences *in vitro* (19, 22, 23). These findings led us to hypothesize that SYNCRIP is a component of the mRNA granules in neuronal dendrites.

To test this hypothesis, we investigated the expression pattern and dynamics of SYNCRIP in the dendrites of rat hippocampal neurons. Expression of SYNCRIP within the hippocampus of rats was investigated by immunohistochemistry using anti-SYCNRIP-N antibodies. SYNCRIP was expressed in the pyramidal cell layer and granular cell layer (Fig. 2*A*), and SYNCRIP signals were mainly observed in the cell bodies of hippocampal neurons (Fig. 2*B*). In addition, the proximal dendrites of pyramidal cells were also labeled with the SYNCRIP antibody (Fig. 2*B*, *arrowheads*). To investigate the localization and dynamics of SYNCRIP in detail, we transfected cultured rat hippocampal neurons with plasmid DNAs encoding mouse SYNCRIP (19) tagged with GFP (GFP-SYNCRIP). To confirm that GFP-SYNCRIP reflects the localization of endogenous SYNCRIP in cultured hippocampal neurons, we compared the immunocytochemical patterns of endogenous SYNCRIP and

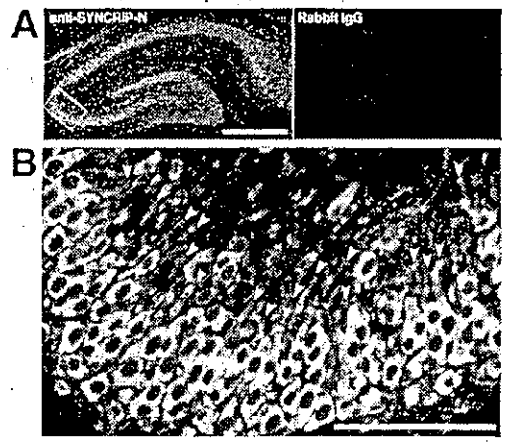

FIG. 2. **Distribution pattern of endogenous SYNCRIP in rat hippocampus.** *A*, *left*, immunohistochemistry with anti-SYNCRIP-N antibody. *Right*, control experiment using nonspecific rabbit IgG. Strong signals for endogenous SYNCRIP were found in the pyramidal and granular layers. *Scale bar*, 500 μm. *B*, a high magnification image of the *boxed* region in *A*. As well as the cell bodies, proximal dendrites of pyramidal neurons were also labeled by anti-SYNCRIP-N antibody (*arrowheads*). Images were taken with a confocal microscope. *Scale bar*, 100 μm.

the distribution of GFP-SYNCRIP signals. Endogenous SYNCRIP was distributed in the dendrites as well as in the cell body of cultured hippocampal neurons (Fig. 3*A*, *left*) as was observed in native tissue. SYNCRIP was found in granules of various sizes in the dendrites (Fig. 3*A*, *right*, *arrowheads*). GFP-SYNCRIP also exhibited a distribution pattern very similar to that of endogenous SYNCRIP (Fig. 3*B*), indicating that the expression pattern of GFP-SYNCRIP reliably reflects that of endogenous SYNCRIP in cultured neurons.

Time-lapse microscopy with a CCD camera revealed that some of the granules labeled with GFP-SYNCRIP traveled within the dendrites (Fig. 4*A* and supplemental Movie 1). Granules labeled with GFP-SYNCRIP moved along the dendrite in both anterograde (to the periphery) and retrograde (to the soma) directions, and a change in direction of movement was observed in some granules (Fig. 4*B*). Double labeling of GFP-SYNCRIP with Texas Red-dextran, which is a marker for endosomes and lysosomes, indicated that the mobile GFP-SYNCRIP-positive granules were not part of the endosome-lysosomal system because GFP-SYNCRIP did not overlap with the Texas Red-dextran signal in either the cell bodies or the dendrites (data not shown). The velocity profile of the GFP-SYN-

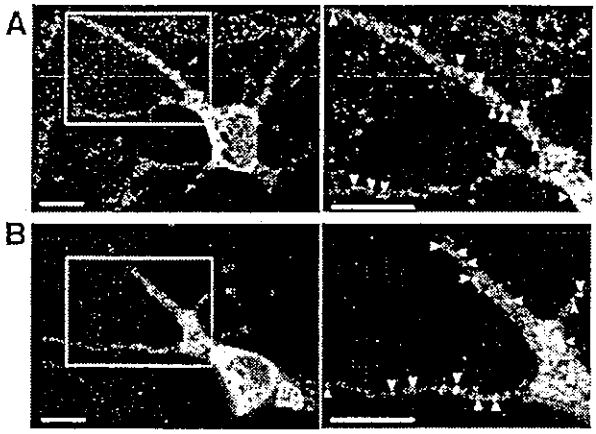

FIG. 3. **The endogenous SYNCRIP protein and expressed GFP-SYNCRIP showed comparable expression patterns in cultured rat hippocampal neurons.** *Right images* are high magnification images of the *boxed region* in the *left images*. *A*, immunolabeling of endogenous SYNCRIP using anti-SYNCRIP-N antibody. *B*, a living cell expressing GFP-SYNCRIP. In both images, many granular structures were observed in dendrites (*arrowheads*). All the images were taken with a confocal microscope. *Scale bars*, 10 μm.

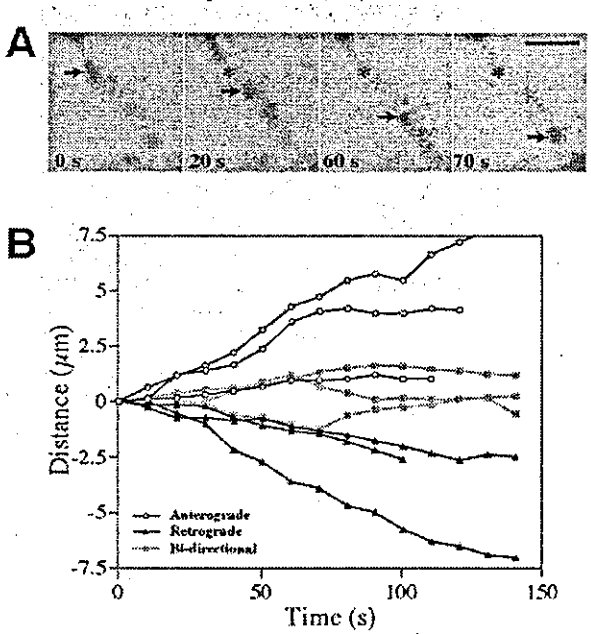

FIG. 4. **Movement of GFP-SYNCRIP-positive granules.** *A*, time-lapse imaging of GFP-SYNCRIP-positive granules in the dendrite recorded with a CCD camera. *Arrows* indicate a moving granule, and *asterisks* indicate the original position of the granule at 0 s. *Scale bar*, 2 μm. *B*, representative movement patterns of GFP-SYNCRIP-positive granules. The net movement of each vesicle (μm) was plotted against time (s). *Anterograde* (positive direction) is the movement from the cell body toward the periphery, and *Retrograde* (negative direction) is the opposite movement. The time-lapse interval was 10 s.

CRIP-positive granules is shown in Fig. 5 (*No drug treatment*). The average velocity of the vesicle movements was about 0.05 μm/s in both the anterograde and retrograde directions as shown in Table I, and the maximum velocity of GFP-SYNCRIP movement was 0.37 μm/s. Interestingly, the speed of SYNCRIP movement was similar to that reported for mRNA granule movement (~0.1 μm/s (9); ~0.1 μm/s (37); 0.03~0.05 μm/s (38)).

The movements of mRNA granules have been reported to be

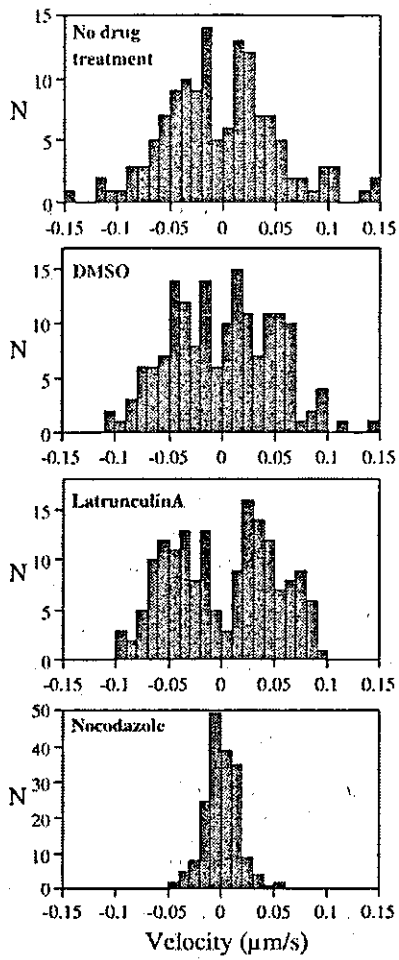

FIG. 5. **Velocity profiles of the GFP-SYNCRIP-positive granules with or without drug treatments.** *N* indicates the number of events, *i.e.* consecutive mono-directional movements. Positive velocity corresponds to the anterograde movement, and negative velocity corresponds to the retrograde movement. *DMSO*, Me_2SO.

mainly dependent on microtubules (9, 18, 35, 37–39). To determine whether microtubules are also involved in the movement of SYNCRIP-positive granules, we tested the effects of drugs that disrupt these cytoskeletal components on the velocity of granule movement. After confirming that these drugs were effective in cultured rat hippocampal neurons by immunocytochemical staining with anti-tubulin antibody (for microtubules) and Alexa 594-phalloidin (for actin filaments) (data not shown), nocodazole (30 μg/ml) and latrunculin A (1 μg/ml) were used to disrupt microtubules and actin filaments, respectively. Neither substance had a major effect on the distribution pattern or number of granules labeled with GFP-SYNCRIP. Latrunculin A did not have a significant effect on the velocity of GFP-SYNCRIP-positive granules in comparison with control cells exposed to 0.3% Me_2SO ($p > 0.1$, *t* test, and Mann-Whitney *U* test). However, nocodazole significantly decreased the velocity of GFP-SYNCRIP-positive granules by ~70% in both directions compared with control cells ($p < 0.001$, *t* test and Mann-Whitney *U* test, Fig. 5 and Table I). These results suggest that the transport of SYNCRIP-positive granules is highly dependent on microtubules and that the contribution of the actin cytoskeleton is minor, which is consistent with previous reports for the transport of mRNA granules.

TABLE I
Effects of drug treatment on the velocity of the movement of GFP-SYNCRIP-positive granules

Drug	Anterograde	Retrograde
	μm/s	*μm/s*
No drug treatment	0.050 ± 0.051 (n = 66)[a]	0.055 ± 0.058 (n = 75)
Me_2SO	0.041 ± 0.028 (n = 84)	0.041 ± 0.025 (n = 79)
Latrunculin A	0.045 ± 0.023 (n = 85)	0.043 ± 0.023 (n = 82)
Nocodazole	0.014 ± 0.010 (n = 90)[b]	0.012 ± 0.009 (n = 89)[b]

[a] Values show average ± S.D.
[b] $p < 0.001$ (t test, Mann-Whitney U test)

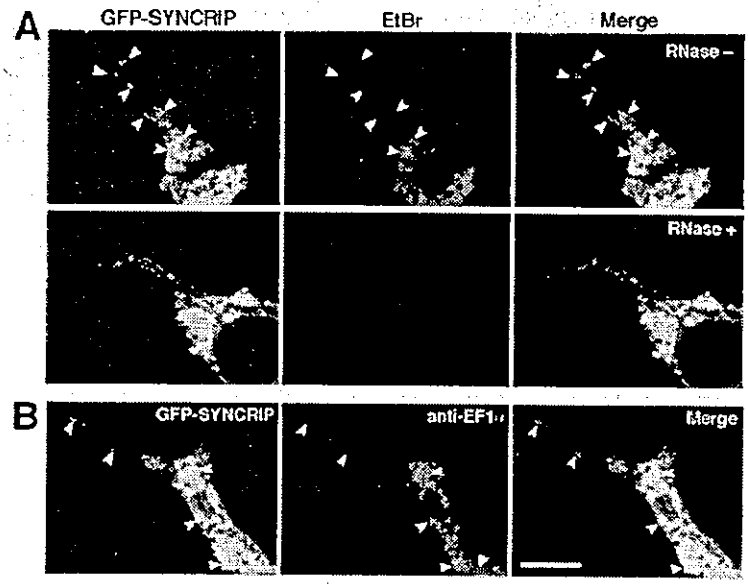

FIG. 6. **The GFP-SYNCRIP protein co-localized with the components of mRNA granules.** *A*, RNA labeling of GFP-SYNCRIP-expressing neurons with EtBr. *Top*, EtBr signals overlapped with GFP-SYNCRIP-positive granules (*arrowheads*). *Bottom*, EtBr signals were abolished by treatment with RNase A. *B*, double-labeling with GFP-SYNCRIP and endogenous EF1α, a marker for mRNA granules. Endogenous EF1α was found on the GFP-SYNCRIP-labeled granules (*arrowheads*). Images were taken with a confocal microscope. The *scale bar* indicates 10 μm.

SYNCRIP Was Co-localized with Dendritic RNAs and Markers of mRNA Granules—We then investigated whether the distribution of SYNCRIP overlaps with that of RNA and mRNA granule markers in dendrites of cultured hippocampal neurons. Dendritic RNAs were labeled with EtBr as described previously (35). The EtBr signal was completely abolished by RNase treatment, indicating that it was specific for RNA (Fig. 6*A*, *bottom*). In the absence of RNase, EtBr labeled granular structures in the cell bodies and dendrites, which overlapped with the most of the SYNCRIP-positive granules (Fig. 6*A*, *top*).

We also investigated whether GFP-SYNCRIP was co-localized with protein components of mRNA granules, *i.e.* EF1α (9) and staufen (15, 40). Immunocytochemistry using anti-EF1α antibody revealed that GFP-SYNCRIP-positive granules were co-localized with endogenous EF1α (Fig. 6*B*). However, we were not able to perform immunocytochemistry for staufen, because no specific antibody against rat staufen was available. Instead, we used GFP-tagged human staufen1 (GFP-hStau1), which is transported within dendrites as a component of mRNA granules (37). GFP-hStau1 was co-expressed with SYNCRIP tagged with monomeric RFP (mRFP-SYCNRIP), whose behavior was indistinguishable from that of GFP-SYNCRIP (data not shown). mRFP-SYNCRIP was co-localized with GFP-hStau1 in granules (Fig. 7*A*), and we confirmed that the GFP-hStau1-positive granules contained endogenous SYNCRIP by immunocytochemistry (supplemental data S1). These results strongly indicate that SYNCRIP is a component of the mRNA granule in neurons.

SYNCRIP Is a Component of Moving mRNA Granules Containing the 3′-UTR of IP_3R1 mRNA—Fig. 7*B* and supplemental Movie 2 show representative time-lapse images of a dendrite from a hippocampal neuron expressing mRFP-SYNCRIP and GFP-hStau1. The mRFP-SYNCRIP signal completely overlapped with that of GFP-hStau1 throughout the movement, indicating that SYNCRIP is a component of the "moving" mRNA granules.

Finally, we investigated whether the SYNCRIP-positive granules actually transport meaningful sets of mRNAs. The mRNA of IP_3R1 is expressed in central nervous system neurons, including hippocampal neurons (41). In addition, IP_3R1 mRNA has been shown to be present in the dendrites of cerebellar Purkinje cells and neocortical neurons (41, 42). Because a sequence homologous to the hnRNP A2 response element (A2RE, GCCAAGGAGCCAGAGAGCATG), which is included in a subset of dendritically localized mRNAs generally transported as components of mRNA granules (18, 43), is found in the 3′-UTR of IP_3R1 mRNA (GCAAATGAGGCAGAGGGACTC, bases identical to those of A2RE are underlined), it is a candidate for a component of mRNA granules. We visualized the 3′-UTR of IP_3R1 mRNA in living neurons by a GFP-based mRNA labeling technique that was first reported in yeast (29) and was used later to visualize several mRNAs in neuronal dendrites (17, 38). We prepared two plasmids, with one (NLS-MS2-Venus) containing the coding sequences of the single-stranded RNA phage capsid protein MS2 fused with Venus (a brighter variant of yellow fluorescent protein (30)) and an NLS. The other plasmid (IP_3R1 3′-UTR-MS2bs) contained 12 repeats of the MS2 binding sequence, each of which encoded a 17-nucleotide RNA stem loop fused with the 3′-UTR of IP_3R1 mRNA (bases 8579–9041). When these plasmids were co-transfected into hippocampal neurons, small bright granules were seen in the dendrites (Fig. 8*A*, *top*), whereas diffuse, not punctate staining was seen in the dendrites in a control experiment in which NLS-MS2-Venus alone was transfected (Fig. 8*A*, *bot-*

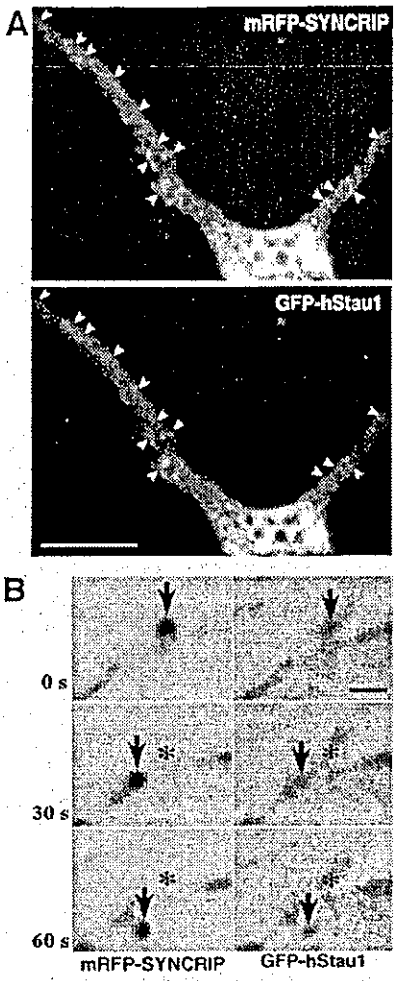

FIG. 7. **mRFP-SYNCRIP proteins were incorporated in motile mRNA granules.** *A*, double labeling of neurons with mRFP-SYNCRIP and GFP-tagged human staufen (GFP-hStau1). mRFP-SYNCRIP and GFP-hStau1 co-localized on the same granules (*arrowheads*). Images were taken with a confocal microscope. *Scale bar*, 10 μm. *B*, time-lapse images of a granule containing mRFP-SYNCRIP and GFP-hStau1 in a dendrite. *Left*, consecutive frames showing a mRFP-SYNCRIP signal. *Right*, corresponding frames showing a GFP-hStau1 signal. *Arrows* indicate a moving granule, and *asterisks* indicate the original position of the granule at 0 s. Note that both mRFP-SYNCRIP and GFP-hStau1 labeled the same moving granule. *Scale bar*, 2 μm.

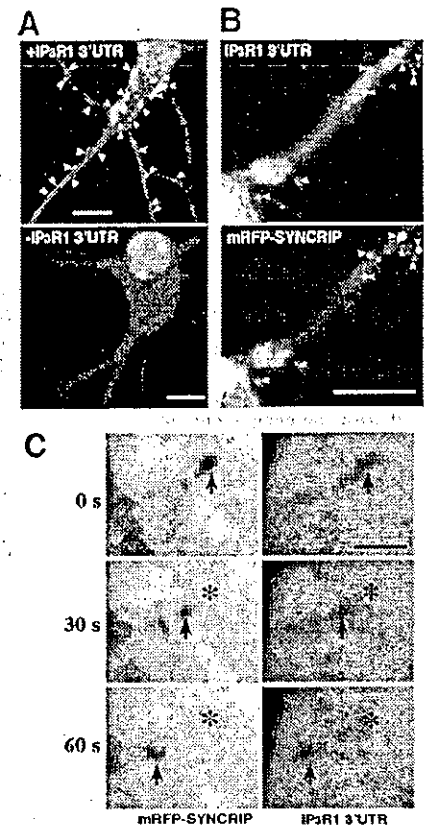

FIG. 8. **3′-UTR of IP_3R1 mRNA was co-transported with mRFP-SYNCRIP.** *A*, to visualize the 3′-UTR of IP_3R1 mRNA, cultured neurons were co-transfected with plasmid DNAs encoding 3′-UTR of mouse IP_3R1 mRNA fused with 12 copies of the MS2 binding sequence (IP_3R1 3′-UTR-MS2bs) and Venus fused with the MS2 and NLS (NLS-MS2-Venus). IP_3R1 3′-UTR mRNAs expressed in neurons was distributed as granular structures (*top*, *arrowheads*). On the other hand, a diffuse staining pattern was observed when NLS-MS2-Venus alone was transfected (*bottom*). *B*, double labeling of cultured neurons with 3′-UTR of IP_3R1 mRNA and mRFP-SYNCRIP. Many of the Venus-positive granules were mRFP-SYNCRIP-positive (*arrowheads*). Images in *A* and *B* were taken with a confocal microscope. *Scale bars*, 10 μm. *C*, movement of a granule containing mRFP-SYNCRIP and 3′-UTR of IP_3R1 mRNA in a dendrite. *Left*, consecutive frames showing a mRFP-SYNCRIP signal. *Right*, corresponding frames showing a 3′-UTR of IP_3R1 mRNA signal detected by Venus. A CCD camera was used. *Arrows* indicate a moving granule, and *asterisks* indicate the original position of the granule at 0 s. Note that both mRFP-SYNCRIP and the 3′-UTR of IP_3R1 mRNA were on the same moving granule. *Scale bar*, 2 μm.

tom). These granules were also labeled with mRFP-SYNCRIP when mRFP-SYNCRIP was further added to the co-transfected plasmids (Fig. 8*B*). A multicolor time-lapse study revealed that the movement of the IP_3R1 3′-UTR mRNA signal coincided with that of the mRFP-SYNCRIP (Fig. 8*C* and supplemental Movie 3). Taken together, these findings indicate that SYNCRIP is a component of mRNA granules that at least transports IP_3R1 mRNA.

DISCUSSION

In the proteomics study we showed that the SYNCRIP-associated complexes in 293EBNA cells contain at least 111 proteins, some of which seem to be responsible for mRNA processing and translation (Fig. 1 and supplemental Table SI). Cytoplasmic ribosomal proteins and RNA binding proteins such as hnRNP A2/B1, zip code-binding protein 1 (IGF-II mRNA-binding protein 1), and hnRNP U, which are the components of mRNA granules (17, 18, 44), were also detected as major SYNCRIP-associated proteins, and this fact raised the possibility that SYNCRIP plays roles as a component of mRNA granules in the neurons. Very recently, a screening study for RNase-sensitive granules that associate with motor protein kinesin revealed that SYNCRIP is one of the components of mRNA transporting granule (44). Moreover, proteomic and immunoelectron microscopic analyses showed that SYNCRIP is included in mRNA granules purified from rat brains.[2] Our new lines of evidence further strengthen these reports that SYNCRIP is a component of mRNA granules. SYNCRIP were distributed in dendrites of hippocampal neurons as a granular structure (Figs. 2 and 3), and the SYNCRIP-containing granules were transported bi-directionally at a speed of ~0.05 μm/s in a microtubule-dependent manner (Fig. 4 and Table I), as was

[2] W. S. Sossin and P. S. McPherson, Montreal Neurological Institute, McGill University, Quebec, Canada, personal communication.

previously reported for mRNA granule dynamics (9, 18, 35, 37–39, 44). SYNCRIP in the dendrite co-localized with RNA and the component of mRNA granules (Figs. 5–7) and was co-transported with IP_3R1 mRNA (Fig. 8). The molecular mechanism underlying the recruitment of SYNCRIP into mRNA granules remains unknown. One possibility is that SYNCRIP interacts with poly(A) or AU-rich regions that are generally present in the 3′ region of mRNAs, as was supported by the fact that SYNCRIP interacts directly with poly(A) and poly(U) *in vitro* (19, 22, 23). Another possibility is that SYNCRIP is bound to mRNA granules as a component of a protein complex as is reported for a human homolog of SYNCRIP in a non-neuronal cell (24). Clarification of the binding relations among the components of mRNA granules may be required to investigate these possibilities.

It is interesting that a number of mitochondrial ribosomal proteins associated with SYNCRIP in 293EBNA cells (Fig. 1 and supplemental Table SI). However, SYNCRIP was not found in mitochondria either in the human kidney cell line and the cultured hippocampal neuron (data not shown). SYNCRIP might associate with mitochondrial ribosomal proteins in the cytoplasm and have indirect roles in protein synthesis in mitochondria, but further study is required to test this possibility.

Microtubule-based motor proteins kinesin and dynein are possibly responsible for the transport of SYCNRIP-positive mRNA granule, since they were co-purified with SYNCRIP-containing mRNA granules (44).[2] mRNA granules that contain cytoplasmic polyadenylation element-binding protein has also been shown to be co-localized with molecular motor kinesin and dynein (39). Bi-directional movement of GFP-SYNCRIP-positive granules (Fig. 4) could be explained by mixed polarity of the dendritic microtubules (45) or by coordination of multiple, opposite-directed motor proteins. In the present study, actin filaments were shown to contribute little to the transport of SYNCRIP (Fig. 5 and Table I), which has also been reported to be the case for the movement of hnRNP A2-positive mRNA granules (18). Although actin filaments seem less involved in the transport of mRNA granules, an actin motor myosin V is shown to be a component of the mRNA/protein complex containing staufen and fragile X mental retardation protein (46). Our results do not necessarily exclude a possible association of SYNCRIP-containing mRNA granules with actin filaments.

The speed of GFP-SYNCRIP-positive granule movement (~0.05 μm/s, Fig. 5) was comparable with that of mRNA granules visualized by SYTO14 (0.1 μm/s, 9), of staufen-containing granules (~0.1 μm/s, 37), and of mRNA granules containing the 3′-UTR of CaMKIIα mRNA (0.03~0.05 μm/s (38)). However, the speed of GFP-SYNCRIP was much slower than that of zip code-binding protein 1 and β-actin mRNA-positive granules, which move at an average velocity of ~1.0 μm/s (17), which exceeds the maximum speed of GFP-SYNCRIP movement (0.37 μm/s). This result suggests a possibility that SYNCRIP is not involved in mRNA granules that are transported at a fast speed. Variety in the transport speeds of mRNA granules may reflect the heterogeneity in mRNA granules that has been proposed recently (47).[2] In addition to the differences in the motor proteins interacting with each subset of mRNA granules, interaction between mRNA granules and organelles may modulate the dynamics of mRNA granules. mRNA granules containing staufen and fragile X mental retardation protein are reported to associate with rough endoplasmic reticulum (46), and this association may affect the transport of mRNA granules. Further work is required to understand the heterogeneity in mRNA granules and their transport.

In this study, we have demonstrated that 3′-UTR of IP_3R1 is co-transported with SYNCRIP as mRNA granules (Fig. 8). Although IP_3R1 mRNA was previously shown to be present in the dendrites of cerebellar Purkinje cells and neocortical neurons (41, 42), the mechanism underlying the dendritic distribution of IP_3R1 mRNA has never been elucidated. This study suggests that IP_3R1 mRNA may be delivered into the dendrites via mRNA granule transport and that 3′-UTR of IP_3R1 mRNA may contain a targeting signal to dendritic mRNA granules, as is known for other dendritic localized mRNAs. IP_3R plays an important role, such as induction of synaptic plasticity in neuronal dendrites (48–50). The dendritic localization and local translation of CaMKIIα mRNA are responsible for the delivery of the kinase and for the induction of synaptic plasticity (51). The dendritic transported mRNA granules containing IP_3R1 mRNA may also be important for accurate delivery of IP_3R1 proteins into the post-synapse and for the induction of synaptic plasticity.

Although the physiological roles of SYNCRIP are still poorly understood even in non-neuronal cells, some interesting properties of SYNCRIP have been reported. Because SYNCRIP is a component of a protein complex that stabilizes c-*fos* mRNA (24), it is possible that SYNCRIP also stabilizes mRNAs during their transport in dendrites. Insulin stimulation and osmotic shocks are reported to induce phosphorylation of tyrosine residues of SYNCRIP, and the RNA binding activity of SYNCRIP is modified by phosphorylation (22, 23). Insulin is present in the brain (for review, see Ref. 52), and insulin receptor tyrosine kinases are abundant in the hippocampus, especially in neuronal dendrites, including synapses (53, 54). In addition, overexpressed fibroblast growth factor receptor 1, a receptor tyrosine kinase that is expressed in hippocampal neurons (55), is also shown to phosphorylate a human homolog of SYNCRIP (NSAP1) on its tyrosine 373, which is located in the third RNA recognition motif domain (56). These studies raise intriguing possibilities that the turnover or translation of mRNAs contained within mRNA granules could be controlled by the insulin- or fibroblast growth factor-dependent phosphorylation of SYNCRIP in hippocampal neurons. Elucidating the functions of SYNCRIP and its regulatory mechanism in mRNA granules may provide an important key for understanding the temporal and spatial regulation of the local translation of mRNA involved in the induction of synaptic plasticity.

Acknowledgments—We thank Dr. R. Tsien (University of California, San Diego, CA) for the gift of monomeric RFP, Dr. S. Sugano (The Institute of Medical Science, The University of Tokyo, Tokyo, Japan) for the gift of a cDNA clone for human staufen1 (HEP22160), Dr. R. Singer (Saint Mary's University, Nova Scotia, Canada) for the gift of pGA14-MS2-GFP, Dr. A. Miyawaki (RIKEN, Saitama, Japan) for the gift of CS2-Venus, and Drs. McPherson and Sossin (Montreal Neurological Institute, McGill University, Quebec, Canada) for valuable discussions. We also thank M. Iwai (The University of Tokyo) for assistance with plasmid construction.

REFERENCES

1. Bashirullah, A., Cooperstock, R. L., and Lipshitz, H. D. (1998) *Annu. Rev. Biochem.* 67, 335–394
2. Kuhl, D., and Skehel, P. (1998) *Curr. Opin. Neurobiol.* 8, 600–606
3. Tiedge, H., Bloom, F. E., and Richter, D. (1999) *Science* 283, 186–187
4. Kiebler, M. A., and DesGroseillers, L. (2000) *Neuron* 25, 19–28
5. Kacharmina, J. E., Job, C., Crino, P., and Eberwine, J. (2000) *Proc. Natl. Acad. Sci. U. S. A.* 97, 11545–11550
6. Aakalu, G., Smith, W. B., Nguyen, N., Jiang, C., and Schuman, E. M. (2001) *Neuron* 30, 489–502
7. Job, C., and Eberwine, J. (2001) *Proc. Natl. Acad. Sci. U. S. A.* 98, 13037–13042
8. Steward, O., and Schuman, E. M. (2003) *Neuron* 40, 347–359
9. Knowles, R. B., Sabry, J. H., Martone, M. E., Deerinck, T. J., Ellisman, M. H., Bassell, G. J., and Kosik, K. S. (1996) *J. Neurosci.* 16, 7812–7820
10. Racca, C., Gardiol, A., and Triller, A. (1997) *J. Neurosci.* 17, 1691–1700
11. Wanner, I., Bander, S. L., Brich, M., Oberdick, J., and Schilling, K. (1997) *Histochem. Cell Biol.* 108, 345–357
12. Tiedge, H., and Brosius, J. (1996) *J. Neurosci.* 16, 7171–7181
13. Torre, E. R., and Steward, O. (1996) *J. Neurosci.* 16, 5967–5978
14. Feng, Y., Gutekunst, C. A., Eberhart, D. E., Yi, H., Warren, S. T., and Hersch, S. M. (1997) *J. Neurosci.* 17, 1539–1547
15. Kiebler, M. A., Hemraj, I., Verkade, P., Köhrmann, M., Fortes, P., Marion, R. M., Ortin, J., and Dotti, C. G. (1999) *J. Neurosci.* 19, 288–297

16. Severt, W. L., Biber, T. U., Wu, X., Hecht, N. B., DeLorenzo, R. J., and Jakoi, E. R. (1999) *J. Cell Sci.* **112**, 3691–3702
17. Tiruchinapalli, D. M., Oleynikov, Y., Kelic, S., Shenoy, S. M., Hartley, A., Stanton, P. K., Singer, R. H., and Bassell, G. J. (2003) *J. Neurosci.* **23**, 3251–3261
18. Shan, J., Munro, T. P., Barbarese, E., Carson, J. H., and Smith, R. (2003) *J. Neurosci.* **23**, 8859–8866
19. Mizutani, A., Fukuda, M., Ibata, K., Shiraishi, Y., and Mikoshiba, K. (2000) *J. Biol. Chem.* **275**, 9823–9831
20. Harris, C. E., Boden, R. A., and Astell, C. R. (1999) *J. Virol.* **73**, 72–80
21. Mourelatos, Z., Abel, L., Yong, J., Kataoka, N., and Dreyfuss, G. (2001) *EMBO J.* **20**, 5443–5452
22. Hresko, R. C., and Mueckler, M. (2000) *J. Biol. Chem.* **275**, 18114–18120
23. Hresko, R. C., and Mueckler, M. (2002) *J. Biol. Chem.* **277**, 25233–25238
24. Grosset, C., Chen, C. Y., Xu, N., Sonenberg, N., Jacquemin-Sablon, H., and Shyu, A. B. (2000) *Cell* **103**, 29–40
25. Yanagida, M., Shimamoto, A., Nishikawa, K., Furuichi, Y., Isobe, T., and Takahashi, N. (2001) *Proteomics* **1**, 1390–1404
26. Natsume, T., Yamauchi, Y., Nakayama, H., Shinkawa, T., Yanagida, M., Takahashi, N., and Isobe, T. (2002) *Anal. Chem.* **74**, 4725–4733
27. Yanagida, M., Hayano, T., Yamauchi, Y., Shinkawa, T., Natsume, T., Isobe, T., and Takahashi, N. (2004) *J. Biol. Chem.* **279**, 1607–1614
28. Campbell, R. E., Tour, O., Palmer, A. E., Steinbach, P. A., Baird, G. S., Zacharias, D. A., and Tsien, R. Y. (2002) *Proc. Natl. Acad. Sci. U. S. A.* **99**, 7877–7882
29. Bertrand, E., Chartrand, P., Schaefer, M., Shenoy, S. M., Singer, R. H., and Long, R. M. (1998) *Mol. Cell* **2**, 437–445
30. Nagai, T., Ibata, K., Park, E. S., Kubota, M., Mikoshiba, K., and Miyawaki, A. (2002) *Nat. Biotechnol.* **20**, 87–90
31. Higgins, D., and Banker, G. (1998) in *Culturing Nerve Cells* (Banker, G., and Goslin, K., eds) pp. 37–78, MIT Press, Cambridge, MA
32. Bannai, H., Inoue, T., Nakayama, T., Hattori, M., and Mikoshiba, K. (2004) *J. Cell Sci.* **117**, 163–175
33. Köhrmann, M., Haubensak, W., Hemraj, I., Kaether, C., Leßmann, V. J., and Kiebler, M. A. (1999) *J. Neurosci. Res.* **58**, 831–835
34. Blanpied, T. A., Scott, D. B., and Ehlers, M. D. (2002) *Neuron* **36**, 435–449
35. Tang, S. J., Meulemans, D., Vazquez, L., Colaco, N., and Schuman, E. (2001) *Neuron* **32**, 463–475
36. O'Brien, T. W. (2002) *Gene (Amst.)* **286**, 73–79
37. Köhrmann, M., Luo, M., Kaether, C., DesGroseillers, L., Dotti, C. G., and Kiebler, M. A. (1999) *Mol. Biol. Cell* **10**, 2945–2953
38. Rook, M. S., Lu, M., and Kosik, K. S. (2000) *J. Neurosci.* **20**, 6385–6393
39. Huang, Y. S., Carson, J. H., Barbarese, E., and Richter, J. D. (2003) *Genes Dev.* **17**, 638–653
40. Mallardo, M., Deitinghoff, A., Muller, J., Goetze, B., Macchi, P., Peters, C., and Kiebler, M. A. (2003) *Proc. Natl. Acad. Sci. U. S. A.* **100**, 2100–2105
41. Furuichi, T., Simon-Chazottes, D., Fujino, I., Yamada, N., Hasegawa, M., Miyawaki, A., Yoshikawa, S., Guenet, J. L., and Mikoshiba, K. (1993) *Receptors Channels* **1**, 11–24
42. Bagni, C., Mannucci, L., Dotti, C. G., and Amaldi, F. (2000) *J. Neurosci.* **20**, 1–6
43. Ainger, K., Avossa, D., Diana, A. S., Barry, C., Barbarese, E., and Carson, J. H. (1997) *J. Cell Biol.* **138**, 1077–1087
44. Kanai, Y., Dohmae, N., and Hirokawa, N. (2004) *Neuron* **43**, 513–525
45. Baas, P. W., Deitch, J. S., Black, M. M., and Banker, G. A. (1988) *Proc. Natl. Acad. Sci. U. S. A.* **85**, 8335–8339
46. Ohashi, S., Koike, K., Omori, A., Ichinose, S., Ohara, S., Kobayashi, S., Sato, T. A., and Anzai, K. (2002) *J. Biol. Chem.* **277**, 37804–37810
47. Duchaine, T. F., Hemraj, I., Furic, L., Deitinghoff, A., Kiebler, M. A., and DesGroseillers, L. (2002) *J. Cell Sci.* **115**, 3285–3295
48. Inoue, T., Kato, K., Kohda, K., and Mikoshiba, K. (1998) *J. Neurosci.* **18**, 5366–5373
49. Fujii, S., Matsumoto, M., Igarashi, K., Kato, H., and Mikoshiba, K. (2000) *Learn. Mem.* **7**, 312–320
50. Nishiyama, M., Hong, K., Mikoshiba, K., Poo, M. M., and Kato, K. (2000) *Nature* **408**, 584–588
51. Miller, S., Yasuda, M., Coats, J. K., Jones, Y., Martone, M. E., and Mayford, M. (2002) *Neuron* **36**, 507–519
52. Wozniak, M., Rydzewski, B., Baker, S. P., and Raizada, M. K. (1993) *Neurochem. Int.* **22**, 1–10
53. Hill, J. M., Lesniak, M. A., Pert, C. B., and Roth, J. (1986) *Neuroscience* **17**, 1127–1138
54. Abbott, M. A., Wells, D. G., and Fallon, J. R. (1999) *J. Neurosci.* **19**, 7300–7308
55. Lin, S. D., and Fann, M. J. (1998) *J. Biomed. Sci.* **5**, 111–119
56. Hinsby, A. M., Olsen, J. V., Bennett, K. L., and Mann, M. (2003) *Mol. Cell. Proteomics* **2**, 29–36

Cell, Vol. 120, 85–98, January 14, 2005. Copyright ©2005 by Elsevier Inc. DOI 10.1016/j.cell.2004.11.048

Subtype-Specific and ER Lumenal Environment-Dependent Regulation of Inositol 1,4,5-Trisphosphate Receptor Type 1 by ERp44

Takayasu Higo,[1,2] Mitsuharu Hattori,[1,3,6] Takeshi Nakamura,[4] Tohru Natsume,[5] Takayuki Michikawa,[1] and Katsuhiko Mikoshiba[1,2,4,*]
[1]Department of Molecular Neurobiology
Institute of Medical Science
University of Tokyo
4-6-1 Shirokanedai, Minato-ku
Tokyo 108-8639
Japan
[2]Laboratory for Developmental Neurobiology
Brain Science Institute
RIKEN, Wako, Saitama 351-0198
Japan
[3]PRESTO
[4]Calcium Oscillation Project
ICORP, JST
Kawaguchi, Saitama 332-0012
Japan
[5]Protein Network Team
Functional Genome Group
Japan Biological Information Research Center
Koto-ku
Tokyo 135-8073
Japan

Summary

Inositol 1,4,5-trisphosphate receptors (IP_3Rs) are intracellular channel proteins that mediate Ca^{2+} release from the endoplasmic reticulum (ER) and are involved in many biological processes and diseases. IP_3Rs are differentially regulated by a variety of cytosolic proteins, but their regulation by ER lumenal protein(s) remains largely unexplored. In this study, we found that ERp44, an ER lumenal protein of the thioredoxin family, directly interacts with the third lumenal loop of IP_3R type 1 (IP_3R1) and that the interaction is dependent on pH, Ca^{2+} concentration, and redox state: the presence of free cysteine residues in the loop is required. Ca^{2+}-imaging experiments and single-channel recording of IP_3R1 activity with a planar lipid bilayer system demonstrated that IP_3R1 is directly inhibited by ERp44. Thus, ERp44 senses the environment in the ER lumen and modulates IP_3R1 activity accordingly, which should in turn contribute to regulating both intralumenal conditions and the complex patterns of cytosolic Ca^{2+} concentrations.

Introduction

The cytosolic Ca^{2+} concentration ($[Ca^{2+}]_C$) is the focal point of many signal transduction pathways and regulates a variety of cellular activities ranging from fertilization to cell death (Berridge et al., 2003). $[Ca^{2+}]_C$ is tightly regulated in terms of time, space, and amplitude, and cells extract specific information based on these parameters. Ca^{2+} ions can be supplied to the cytosol from the extracellular space or from intracellular Ca^{2+} stores, such as the endoplasmic reticulum (ER). Dysfunction of molecules involved in $[Ca^{2+}]_C$ regulation is assumed to play a major role in apoptosis (Orrenius et al., 2003) and neuropathological conditions, including Huntington's and Alzheimer's diseases (Paschen, 2003; Mattson, 2004). Inositol 1,4,5-trisphosphate receptors (IP_3Rs) are Ca^{2+} release channels on the ER that play a critical role in the generation of complex $[Ca^{2+}]_C$ patterning, e.g., Ca^{2+} waves and oscillations (Patterson et al., 2004). There are three IP_3R subtypes in birds and mammals, IP_3R1, IP_3R2, and IP_3R3, and they share basic properties but differ in terms of regulation and distribution (Taylor et al., 1999; Patterson et al., 2004). IP_3R1 is the dominant subtype in the brain (Taylor et al., 1999) and has been implicated in neuronal development (Takei et al., 1998; Xiang et al., 2002), in higher functions of the central nervous system (Inoue et al., 1998; Nishiyama et al., 2000), and in human neuropathology (Tang et al., 2003). A striking feature of IP_3Rs is the presence of very large cytosolic regions, including the IP_3 binding core (Patterson et al., 2004). The channel domain contains six transmembrane domains, and as a result there are three "loops" that reside in the ER lumen (Figure 1A). The third lumenal loop (L3) is the largest and can be divided into two subdomains. The first half, the L3V domain, has highly divergent primary sequences according to the subtype (Figure 1B), while the second half, the L3C domain, which includes the pore-forming region (Patterson et al., 2004), is almost completely conserved among types and species. Interestingly, the primary sequence of the L3V domain of each IP_3R subtype is well conserved among animal species, suggesting that this domain is involved in subtype-specific regulation. However, the function of the L3V domain remains largely unexplored.

It is evident that the intralumenal environment of the ER regulates the function of numerous proteins (Berridge et al., 2003), but how it regulates IP_3R activity remains unclear despite a great deal of research. For example, whether IP_3R is directly regulated by the Ca^{2+} concentration in the ER lumen ($[Ca^{2+}]_{ER}$) is still a matter of debate (Caroppo et al., 2003 and references therein). Calreticulin (CRT), an ER lumenal lectin with high Ca^{2+} binding capacity, regulates IP_3-induced Ca^{2+} release (IICR) (Camacho and Lechleiter, 1995; Roderick et al., 1998), but whether or not this is a direct effect on IP_3R remains unknown because CRT critically regulates the activity of sarcoendoplasmic reticulum Ca^{2+} ATPase (SERCA) 2b (Li and Camacho, 2004). Chromogranins that mainly reside in secretory granules associate with the L3C domain of IP_3Rs and modulate the activities of IP_3Rs (Thrower et al., 2003; Choe et al., 2004). However, the mechanisms by which interactions between chromogranins and IP_3Rs are regulated, and their physiological significance, remain unknown.

*Correspondence: mikosiba@ims.u-tokyo.ac.jp
[6]Present address: Department of Biomedical Science, Graduate School of Pharmaceutical Sciences, Nagoya City University, Mizuho-ku, Nagoya, Aichi 467-8603, Japan.

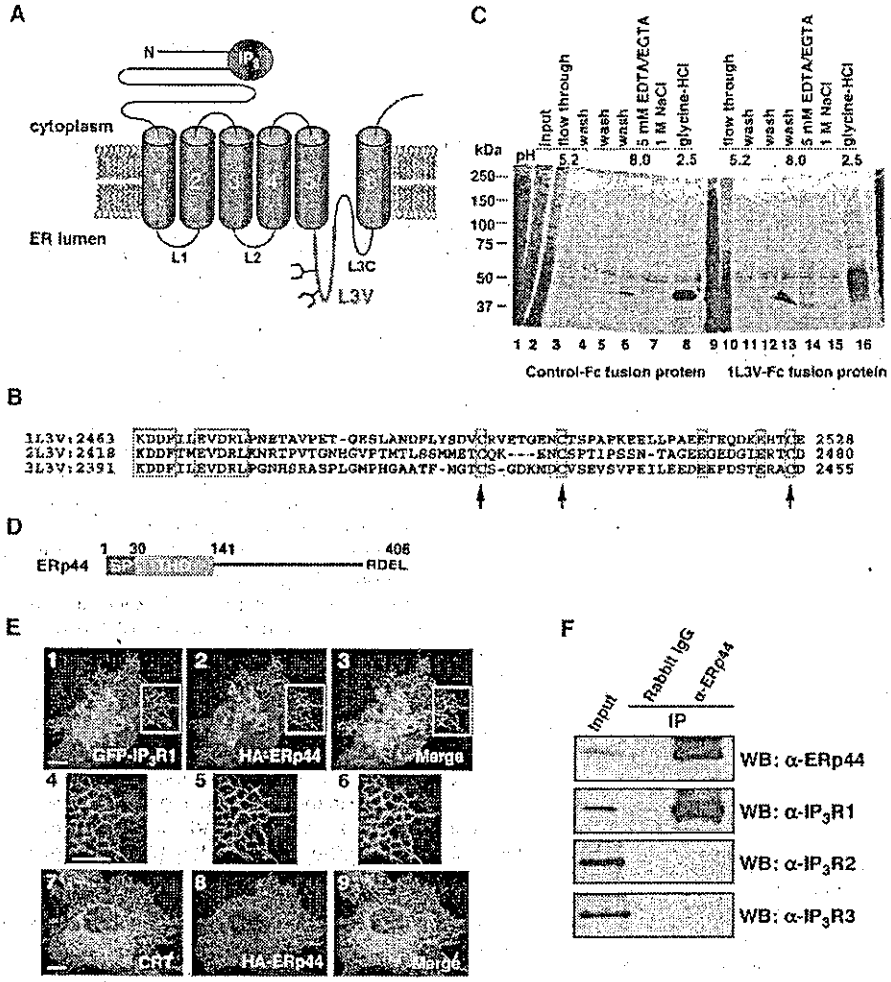

Figure 1. Identification of ERp44 as a Protein Binding to the L3V Domain of IP_3R1

(A) Schematic representation of the structure of IP_3Rs. IP_3Rs contain six membrane-spanning regions (green) and three lumenal domains, L1, L2, and L3. L3 is divided into L3V (red) and L3C. IP_3 binds to the N-terminal cytosolic region. L3V contains two glycosylation sites.

(B) Sequence comparison of the L3V of three subtypes of mouse IP_3R. Conserved amino acid residues are shown (red box). Conserved cysteine residues are indicated by arrows.

(C) Purification of 1L3V-interacting proteins. Mouse cerebellar microsomal fractions solubilized in acidic solution (pH 5.2) were added to either a control-Fc or a 1L3V-Fc column. The columns were washed with the same buffer (lanes 3 and 11), neutral buffer (lanes 4 and 5 and 12 and 13), and finally eluted with neutral buffer containing EGTA/EDTA (lanes 6 and 14), with buffer containing 1M NaCl (lanes 7 and 15), and with glycine-HCl solution (lanes 8 and 16). The arrowhead indicates the 45 kDa band that specifically binds to 1L3V-Fc, and it turned out to be ERp44.

(D) Structure of ERp44. The signal peptide (SP, aa 1–30), thioredoxin homology domain (THD, aa 31–141), and ER retention signal RDEL motif are shown.

(E) ERp44 colocalizes with IP_3R1 in the ER. COS-7 cells expressing HA-ERp44 and GFP-IP_3R1 were stained with α-HA (panels 1–3). The boxed regions in panels 1–3 are shown at increased magnification in panels 4–6, respectively. The cells expressing HA-ERp44 were stained with α-CRT and α-HA (panels 7–9). Scale bar, 10 μm.

(F) In vivo interaction between ERp44 and IP_3R1. HeLa cells were treated with a membrane-permeable crosslinker, DSP, and then solubilized. The cell lysates were subjected to IP with control rabbit IgG or α-ERp44. The lysate (Input) and IP samples were analyzed by Western blotting (WB) with indicated antibodies.

To elucidate the molecular mechanism underlying subtype-specific regulation of IP_3Rs on the ER lumen side, we searched for proteins that bind to the L3V domain of IP_3Rs. We succeeded in identifying ERp44, a thioredoxin (TRX) family protein previously implicated in oxidative protein folding, as a protein that specifically binds to the L3V domain of IP_3R1. Herein, we present strong evidence that ERp44 directly inhibits the channel activity of the IP_3R1 in a pH-, redox state-, and $[Ca^{2+}]_{ER}$-dependent manner. This is the first demonstration of negative regulation of IP_3Rs by a specific binding protein in the ER lumen. We anticipate that our results will contribute to understanding of the mechanism by which cells integrate various signals from the extracellular mi-

lieu and from the ER lumen in generating complex Ca^{2+} signaling patterns.

Results

Identification of ERp44 as a Binding Protein of the L3V Domain of IP_3R1

Our first goal was to identify proteins that bind to the L3V domain of IP_3Rs. Yeast two-hybrid screening was considered inappropriate as a method because the chemical conditions in the nucleus are completely different from those in the ER lumen. We therefore produced 1L3V-Fc protein by fusing the secretion signal and human immunoglobulin Fc domain to the N and C termini, respectively, of the L3V domain of IP_3R1 (1L3V) and then used it to prepare affinity resin. When an initial attempt under neutral conditions (pH 7.5, data not shown) failed to detect any specific 1L3V-Fc binding protein in the mouse cerebellar microsomal fraction, we performed a similar experiment under acidic conditions (pH 5.2) and succeeded in identifying two proteins that bound specifically to 1L3V-Fc (Figure 1C). Analysis of the bands by matrix-assisted laser desorption/ionization-time of flight mass spectrometry revealed the 44 kDa protein to be ERp44 (Anelli et al., 2002). The 85 kDa protein was identified as aconitase, a mitochondrial protein, and was not further characterized in this study. We then searched for binding proteins for the L3 domains of IP_3R2 and IP_3R3 (2L3V or 3L3V, respectively) in mouse brain, employing the same procedures, but detected none (data not shown).

ERp44 is an ER lumenal protein of the TRX family and contains a signal peptide, TRX-homology domain (THD), and an ER retention signal, RDEL (Figure 1D). ERp44 is widely expressed in mouse tissues (Supplemental Figure S1 at http://www.cell.com/cgi/content/full/120/1/85/DC1/). Hemagglutinin A epitope (HA)-tagged ERp44 (Anelli et al., 2002), alone or with GFP-IP_3R1, was expressed in COS-7 cells (Figure 1E). HA-ERp44 was observed as a diffuse network with GFP-IP_3R1 and endogenous CRT (Figure 1E), indicating that ERp44 colocalizes with IP_3R1 in the ER.

To confirm the interaction between IP_3R1 and ERp44, we raised polyclonal antibody against ERp44 and conducted immunoprecipitation (IP) experiments. Both IP_3R1 and ERp44 were, however, severely degraded when whole-cell lysates were prepared with acidic buffer (in which an association had been observed in the experiments shown in Figure 1C), presumably by lysosomal proteases (data not shown). To circumvent this, HeLa cells were first treated with a membrane-permeable crosslinker, dithiobis[succinimidylpropionate] (DSP), and IP was performed in neutral buffer. Under these conditions, anti-ERp44 antibody coprecipitated IP_3R1, but not IP_3R2 or IP_3R3 (Figure 1F), indicating that endogenous ERp44 and IP_3R1 exist in the same complex in vivo.

ERp44 Specifically Interacts with IP_3R1, but Not with IP_3R2 or IP_3R3, in a Condition-Dependent Manner

To further characterize the association between ERp44 and IP_3Rs, we performed a series of pulldown experiments with recombinant proteins. Glutathione (GSH) *S*-transferase (GST) and maltose binding protein (MBP) were fused to 1L3V and ERp44, respectively (Figure 2A). Under acidic conditions (pH 5.2), MBP-ERp44 specifically interacted with GST-1L3V (Figure 2B), but no interaction was observed under neutral (pH 7.2) conditions (data not shown). The pH in the ER lumen has been estimated to be almost neutral (Kim et al., 1998; Foyouzi-Youssefi et al., 2000). We reasoned that certain factor(s) may have been missed in our pulldown assays and attempted to identify conditions under which 1L3V and ERp44 interact at neutral pH.

The presence of THD in ERp44 suggests that its function is redox dependent. Both GST-1L3V and ERp44 were predominantly in their oxidized forms, and addition of the reducing reagent dithiothreitol (DTT) reduced both according to their migration patterns on SDS-PAGE under nonreducing conditions (Figure 2C). No interaction between these oxidized forms was observed at pH 7.5 (Figure 2C, lane 1), while the reduced forms did interact (Figure 2C, lane 2). It was thus concluded that ERp44 and 1L3V bind to each other in a redox-dependent manner at neutral pH.

To determine which of the protein redox states is important, the cysteine residues of the proteins were mutated. Mutation of Cys2496, Cys2504, or Cys2527 of 1L3V resulted in decreased interaction with ERp44 (Figure 2D), whereas no cysteine mutations in ERp44 affected the interaction (Supplemental Figure S2 on the *Cell* website). Taken together, these findings strongly suggest that the presence of free thiol groups in 1L3V is required for the interaction between 1L3V and ERp44 at neutral pH.

We next examined whether the interaction between ERp44 and 1L3V is dependent on the Ca^{2+} concentration. As shown in Figure 2E, the interaction diminished when the Ca^{2+} concentration was higher than 100 μM. The $[Ca^{2+}]_{ER}$ under resting conditions has been estimated to be 200–1000 μM (Meldolesi and Pozzan, 1998), suggesting that the interaction between ERp44 and IP_3R1 is enhanced when $[Ca^{2+}]_{ER}$ is decreased.

The above findings suggested that reducing and/or low $[Ca^{2+}]_{ER}$ conditions favor the interaction between ERp44 and IP_3R1. To corroborate these observations in vivo, COS-7 cells expressing HA-ERp44 and GFP-IP_3R1 were cultured in the presence or absence of DTT, and IP was performed with whole-cell lysates. Although the amount of HA-ERp44 that precipitated with anti-HA antibody was consistently less under reducing conditions for unknown reasons (Figure 2F, bottom panel), coprecipitated GFP-IP_3R1 was significantly increased (Figure 2F, middle panel). In a similar manner, cells expressing HA-ERp44 and GFP-IP_3R1 were stimulated with 10 μM (suprathreshold concentration) ATP, an activator of purinergic receptors, and the stimulation increased the amount of GFP-IP_3R1 that coprecipitated with HA-ERp44 (Figure 2G). Furthermore, Ca^{2+} depletion from the ER, elicited by thapsigargin (Tg, a SERCA inhibitor), also augmented the interaction (Figure 2H). These results indicated that dynamic changes in the ER lumenal environment affect the interaction between IP_3R1 and ERp44.

Next, to gain greater insight into the nature of the interaction, we identified the minimum 1L3V-interacting